

Marine Pollution Bulletin

From lipophilic to hydrophilic toxin producers: phytoplankton succession driven by an atmospheric river in western Patagonia

--Manuscript Draft--

Manuscript Number:	
Article Type:	Research Paper
Keywords:	: Pseudo-nitzschia calliantha; lipophilic toxins; amnesic shellfish poisoning; domoic acid; hydro-climatic modulation; Patagonian fjord system
Corresponding Author:	Patricio A Díaz, PhD Puerto Montt, Los Lagos CHILE
First Author:	Patricio A Díaz, PhD
Order of Authors:	Patricio A Díaz, PhD Gonzalo Álvarez, PhD Rosa I. Figueroa, PhD Rene Garreaud, PhD Iván Pérez-Santos, PhD Camila Schwerter, Marine Biologist Manuel Díaz, Naval Engineer Loreto López, Aquaculture Engineer Marco Pinto-Torres, PhD Bernd Krock, PhD
Abstract:	Phytoplankton succession is related to hydroclimatic conditions. In this study we provide the first description of a toxic phytoplankton succession in the Patagonian Fjord System. The shift was modulated by atmospheric-oceanographic forcing and consisted of the replacement of the marine dinoflagellate <i>Dinophysis acuta</i> in a highly stratified water column during austral summer by the diatom <i>Pseudo-nitzschia calliantha</i> in a mixed water column during late summer and early autumn. This transition, accompanied by a change in the biotoxin profiles (from lipophilic dinophysis toxins to hydrophilic domoic acid), was induced by the arrival of an intense atmospheric river. The winds in Magdalena Sound may have been further amplified, due to its west-east orientation and its location within a tall, narrow mountain canyon. This work also documents the first known appearance of toxic <i>P. calliantha</i> in Northern Patagonian. The potential impacts of the biotoxins of this species on higher trophic levels are discussed.
Suggested Reviewers:	Antonella Luglié, PhD University of Sassari luglie@uniss.it Dr. Antonella Luglié (University of Sassari) is an internationally recognised expert in phytoplankton ecology with focus on harmful algal blooms. She has a long career and many publications on the topic, many of them focusing on the noxious and toxic phytoplankton species. Emilio Marañón, PhD University of Vigo em@uvigo.es Dr. Emilio Marañón (Universidade de Vigo) has a long career focused in ecology and biogeochemical role of phytoplankton. His studies focus on phytoplankton diversity and community structure. Marina Montresor, PhD Zoological Station Anton Dohrn

marina.montresor@szn.it

The research interests of Dr. Montresor focus on the diversity and ecology of marine phytoplankton, with particular attention on life histories of microalgae, including species of the genus *Pseudo-nitzschia*. These organisms have multiphasic life cycles that include dormant and sexual phases, which have implications for the dynamics and genetic structure of their populations.

Puerto Montt, April 18, 2023

Dr. Francois Galgani
Editor-in-Chief
Marine Pollution Bulletin

Dear Editor:

Attached, please, find a submission of our original manuscript entitled: “**From lipophilic to hydrophilic toxin producers: phytoplankton succession driven by an atmospheric river in western Patagonia**”, that we would like you to consider for publication in *Marine Pollution Bulletin*.

Harmful Algal Blooms (HABs) constitute a worldwide problem, affecting aquatic ecosystems, public health and local economies. In the last decades, this problem appears to have increased in frequency, geographic extent and intensity due to the increase in nutrient discharges and climate variability, forcing affected sectors, as those related to the aquaculture industry, to think proactive strategies in order to avoid the increasing economic losses. The fjords system in the Chilean Patagonia, are model scenarios for the study of physical-biological interactions during HABs development. So far, most efforts in the country went to monitoring and management of the events and very little field work has been carried out with research purposes.

In the present paper, we describe for the first time a toxic phytoplankton succession in the Patagonian Fjord System (Puyuhuapi Fjord, Aysén Region) modulated by atmospheric-oceanographic forcing (Atmospheric River). The response of a phytoplankton community dominated by *Dinophysis acuta* (dinoflagellate) changing to one dominated by *Pseudo-nitzschia calliantha* (diatom) and the potential impact of its associated toxins on higher trophic levels is widely discussed. In addition, this work also documents the first known appearance of toxic *P. calliantha* in Northern Patagonian.

Our results contribute to a better understanding of HABs in the region and demonstrate the importance of hydroclimatic conditions in the toxic phytoplankton succession in a global “hotspot”, which may alleviate their economic impact in the southern austral region and elsewhere.

We hope you find this contribution of interest for your journal.

Yours sincerely,

Dr. Patricio A. Díaz
E-mail: patricio.diaz@ulagos.cl

Highlights

- Toxic phytoplankton succession modulated by intense atmospheric river in northern Patagonia
- Transition from lipophilic dinophysins toxins to hydrophilic domoic acid.
- The first known appearance of toxic *Pseudo-nitzschia calliantha* in Northern Patagonian.

1
2
3
4
5 1 From lipophilic to hydrophilic toxin producers: phytoplankton succession driven by
6 2 an atmospheric river in western Patagonia
7
8
9 3

10 4 Patricio A. Díaz ^{a,b*}, Gonzalo Álvarez ^{c,d,e}, Rosa I. Figueroa ^f, Rene Garreaud ^{g,h},
11 5 Iván Pérez-Santos ^{a,i,j}, Camila Schwerter ^a, Manuel Díaz ^k, Loreto López ^l,
12 6 Marco Pinto-Torres ^{m,n}, Bernd Krock ^{i,o}
13 7

16 8 ^a Centro i~mar, Universidad de Los Lagos, Casilla 557, Puerto Montt, Chile

17 9 ^b CeBiB, Universidad de Los Lagos, Casilla 557, Puerto Montt, Chile

19 10 ^c Facultad de Ciencias del Mar, Departamento de Acuicultura, Universidad Católica del Norte,
20 11 Coquimbo 1281, Chile

22 12 ^d Centro de Investigación y Desarrollo Tecnológico en Algas (CIDTA), Facultad de Ciencias
23 13 del Mar, Larrondo 1281, Universidad Católica del Norte, Coquimbo, Chile

25 14 ^e Center for Ecology and Sustainable Management of Oceanic Islands (ESMOI),
26 15 Departamento de Biología Marina, Facultad de Ciencias del Mar, Universidad Católica del
27 16 Norte, Coquimbo, Chile

29 17 ^f Centro Oceanográfico de Vigo, Instituto Español de Oceanografía (IEO-CSIC), Vigo, Spain

30 18 ^g Centro de Ciencia del Clima y la Resiliencia (CR2), Universidad de Chile, Chile

32 19 ^h Departamento de Geofísica, Universidad de Chile, Santiago, 8370449, Región
33 20 Metropolitana, Chile

35 21 ⁱ Centro de Investigación Oceanográfica COPAS COASTAL, Universidad de Concepción,
36 22 Concepción, Chile

37 23 ^j Centro de Investigaciones en Ecosistemas de la Patagonia (CIEP), Coyhaique, Chile

39 24 ^k Instituto de Acuicultura, Programa de Investigación Pesquera, Universidad Austral de Chile,
40 25 Los Pinos S/N, Puerto Montt, Chile

42 26 ^l Centro de Estudios de Algas Nocivas (CREAN), Instituto de Fomento Pesquero (IFOP),
43 27 Padre Harter 574, Puerto Montt, Chile

44 28 ^m Programa de Doctorado en Ciencias de la Acuicultura, Universidad Austral de Chile, Los
45 29 Pinos S/N, Puerto Montt, Chile

47 30 ⁿ Centro FONDAP de Investigación de Ecosistemas de Altas Latitudes (IDEAL), Universidad
48 31 Austral de Chile, Av. El Bosque 01789, Punta Arenas, Chile

50 32 ^o Alfred Wegener Institut-Helmholtz Zentrum für Polar- und Meeresforschung, Am
51 33 Handelshafen 12, 27570 Bremerhaven, Germany
52 34

54 35
55 36 *Corresponding author: Patricio A. Díaz

57 37 Centro i~mar & CeBiB, Universidad de Los Lagos, Casilla 557, Puerto Montt, Chile

59 38 Tel: +56-65-2322423; Email: patricio.diaz@ulagos.cl
60
61
62
63
64
65

1
2
3
4
5
6
7
8
9
10
11
12
13
14
15
16
17
18
19
20
21
22
23
24
25
26
27
28
29
30
31
32
33
34
35
36
37
38
39
40
41
42
43
44
45
46
47
48
49
50
51
52
53
54
55
56
57
58
59
60
61
62
63
64
65

39 **Abstract**

40 Phytoplankton succession is related to hydroclimatic conditions. In this study we provide the first
41 description of a toxic phytoplankton succession in the Patagonian Fjord System. The shift was
42 modulated by atmospheric-oceanographic forcing and consisted of the replacement of the marine
43 dinoflagellate *Dinophysis acuta* in a highly stratified water column during austral summer by the
44 diatom *Pseudo-nitzschia calliantha* in a mixed water column during late summer and early autumn.
45 This transition, accompanied by a change in the biotoxin profiles (from lipophilic dinophysis toxins
46 to hydrophilic domoic acid), was induced by the arrival of an intense atmospheric river. The winds
47 in Magdalena Sound may have been further amplified, due to its west-east orientation and its
48 location within a tall, narrow mountain canyon. This work also documents the first known
49 appearance of toxic *P. calliantha* in Northern Patagonian. The potential impacts of the biotoxins
50 of this species on higher trophic levels are discussed.

51
52 **Keywords:** *Pseudo-nitzschia calliantha*; lipophilic toxins; amnesic shellfish poisoning; domoic
53 acid; hydro-climatic modulation; Patagonian fjord system

1. Introduction

Chilean Patagonia is a vast geographical zone that extends nearly 1,500 km (42°S–55°S), covers an area of 240,000 km² and has a coastline of almost 80,000 km (Försterra, 2009). It constitutes a complex system of fjords, channels, gulfs, estuaries and bays and is affected by physical regimes that strongly modulate biological productivity (Iriarte et al., 2014). Harmful algal blooms (HABs) of the toxic dinoflagellate *Alexandrium catenella*, associated with the production of paralytic shellfish toxins (PST), are a frequent occurrence in this region (Díaz et al., 2014; Díaz et al., 2022b; Guzmán et al., 2002; Molinet et al., 2003; Molinet et al., 2010), but HABs of *Dinophysis acuta* and *D. acuminata*, associated with the production of the lipophilic compounds okadaic acid (OA), dinophysistoxins (DTX), and pectenotoxins (PTX) (Baldrich et al., 2021; Contreras and García, 2019; Díaz et al., 2022a; Díaz et al., 2021; García et al., 2012), and of *Protoceratium reticulatum*, associated with the production of yessotoxins (Alves de Souza et al., 2014), have also been reported. Local detections of these marine biotoxins have led to bans on the harvest of natural populations of different bivalve and gastropod species, in addition to interrupting aquaculture efforts, mainly for the mussel *Mytilus chilensis*, in the Aysén and Magallanes regions (Díaz et al., 2019). Ecosystem impacts in Chilean Patagonian waters associated with PST include the mass stranding of marine invertebrates in Cucao Bay, Chiloe Island (42° 38'S–74° 07'W) (Álvarez et al., 2019) and the mass mortality of Sei whales in Penas Gulf (46–48°S) (Häussermann et al., 2017). Biological processes occur under a wide variety of spatial and temporal scales and should thus be studied at the same spatial and temporal scales as the physical-chemical processes with which they interact (GEOHAB, 2010). The formation, maintenance and dissipation of HABs are subject to processes operating at multiple (macro-, meso-, micro-) scales (sensu Haury et al., 1978), all of which are exacerbated in highly heterogeneous systems such as the Patagonian fjord system (PFS),

1
2
3
4
5 77 where multiple niches promote the development or aggregation of different HAB species (Baldich
6
7
8 78 et al., 2023; Baldrich et al., 2021).

9
10 79 The variability of atmospheric processes is one of the main drivers of the hydrodynamics in coastal
11
12
13 80 and shelf areas, particularly in fjord systems. In the PFS, the wind, together with the tide, is one of
14
15 81 the main sources of forcing, but it varies considerably, including at different time scales, due to
16
17
18 82 atmospheric oscillations (Valle-Levinson, 2010; Valle-Levinson and Blanco, 2004). Thus, during
19
20 83 the period of highest biological production (spring–summer) in the PFS, changes in the position of
21
22
23 84 high-low pressure systems result in short-term variations (time scales of a few days) in the wind
24
25 85 regime that promote cycles of stratification-mixing of the water column (Iriarte et al., 2007;
26
27 86 Montero et al., 2011; Pérez-Santos et al., 2021; Pérez-Santos et al., 2019) and thereby modulate
28
29
30 87 the seasonal succession of phytoplanktonic species, including those that cause HABs (Montero et
31
32 88 al., 2017; Pérez-Santos et al., 2021).

33
34 89 The phytoplankton community is generally dominated by diatoms (Iriarte et al., 2007; Pizarro et
35
36
37 90 al., 2005). In the PFS, the increase in the input of nutrients and in light availability that mark the
38
39
40 91 end of winter and the beginning of spring activates phytoplankton activity, evidenced by blooms
41
42 92 dominated by diatoms of the genus *Skeletonema*. In summer, when nutrients are depleted from the
43
44 93 surface waters, phytoplankton sink as they follow the decaying nutrients until light becomes a co-
45
46
47 94 limiting factor (1% of surface photosynthetically active radiance). The resulting subsurface
48
49 95 chlorophyll *a* maximum coincides with the nutricline and the dominance of the diatom genus
50
51 96 *Pseudo-nitzschia*. During mid- to late summer and early autumn, characterized by a high
52
53
54 97 thermohaline stratification driven by extreme climatic anomalies (high pressure/temperature and
55
56
57 98 low wind/rainfall), the phytoplankton community becomes dominated by dinoflagellates (Díaz et
58
59 99 al., 2021) or phytoflagellates (Díaz et al., 2023; León-Muñoz et al., 2018).

1
2
3
4
5
6
7
8
9
10
11
12
13
14
15
16
17
18
19
20
21
22
23
24
25
26
27
28
29
30
31
32
33
34
35
36
37
38
39
40
41
42
43
44
45
46
47
48
49
50
51
52
53
54
55
56
57
58
59
60
61
62
63
64
65

100 In this work, we provide the first description of a succession of toxic phytoplankton species in the
101 PFS (Puyuhuapi Fjord, Aysén region) that was modulated by atmospheric-oceanographic forcing,
102 with a community dominated by the dinoflagellate *D. acuta* replacing one dominated by the diatom
103 *P. calliantha*. This change in community composition and the potential impact of the change in the
104 associated toxins on higher trophic levels are discussed in detail.

2. Material and methods

2.1. Study area and climate background

108 Puyuhuapi Fjord, at 100 km one of the world's most extended fjord and channel systems (Fig. 1)
109 (Pantoja et al., 2011), has an irregular bathymetry and a complex coastal morphology. The mean
110 depth of its waters is 220 m, with a maximum of 350 m close to the mouth of Magdalena Sound
111 (Fig. 1). The marked water column stratification is determined by freshwater input and by seasonal
112 and latitudinal precipitation patterns, which include rainfall and ice melting (Pickard, 1971;
113 Schneider et al., 2014). The primary freshwater input is from the Cisnes River (mean annual
114 discharge $\sim 218 \text{ m}^3 \text{ s}^{-1}$, with peaks $>500 \text{ m}^3 \text{ s}^{-1}$), located in the middle of the fjord. The climate of
115 northwestern Patagonia, including Puyuhuapi Fjord, is temperate and humid, as recurrent mid-
116 latitude depressions embedded in the westerly wind belt (WWB) cause precipitation levels of
117 3500–4000 mm, occurring over 200 days per year (Sauter, 2020) along the coast but in some years
118 reaching ~ 5000 mm inland due to the orographic uplift of the austral Andes (Viale and Garreaud,
119 2015). Many storms that reach northwestern Patagonia feature atmospheric rivers (ARs), defined
120 as long filaments of high moisture transport (Viale et al., 2018) that connect the tropical oceans
121 with mid-latitudes. Global and regional studies indicate that ARs frequently make landfall along
122 the coast of southern Chile and their interaction with the Andes results in even more intense

1
2
3
4
5
6
7
8
9
10
11
12
13
14
15
16
17
18
19
20
21
22
23
24
25
26
27
28
29
30
31
32
33
34
35
36
37
38
39
40
41
42
43
44
45
46
47
48
49
50
51
52
53
54
55
56
57
58
59
60
61
62
63
64
65

123 precipitation events (>100 mm/day), abundant freshwater drainage (Valenzuela and Garreaud,
124 2019) and strong westerly winds.

125
126 **2.2. Climate data**

127 Rainfall, air temperature and river discharge data were obtained from Climate Explorer
128 (<http://explorador.cr2.cl/>), which compiles quality-controlled records from the Chilean Weather
129 Service (DMC) and Water Agency (DGA). Due to the low density of climate stations in Patagonia,
130 additional data from the CR2Met dataset, comprising monthly gridded ($0.05^\circ \times 0.05^\circ$ lat-lon)
131 precipitation and temperature fields over Chile from 1979 to date, were also used. CR2Met was
132 built by the optimal interpolation of surface data using state-of-the-art European Centre reanalysis
133 data (Álvarez-Garreton et al., 2018). The large-scale circulation during early 2018 was
134 characterized using the ERA5 reanalysis of the European Centre for Medium-Range Weather
135 Forecasts (Hersbach et al., 2020), with an hourly resolution on a $0.25^\circ \times 0.25^\circ$ lat-lon grid and 137
136 vertical levels. The data were obtained through the Copernicus Climate Data Store archive
137 (<https://cds.climate.copernicus.eu/>).

138
139 **2.3. Field sampling**

140 During summer and early autumn 2018, four one-day cruises of the *RV Queen* were carried out in
141 the Puyuhuapi fjord area, Chilean Patagonia: on January 17, February 22, March 12 and April 24.
142 On every cruise, samples were taken at a fixed sampling station located at the head of Magdalena
143 Sound, to measure the physical-chemical properties of the water column and the fine-scale
144 distribution of phytoplankton, with a focus on toxic species (Fig. 1).

1
2
3
4
5 145 Vertical profiles of temperature, salinity and *in vivo* chlorophyll *a* fluorescence were obtained using
6
7
8 146 an AML Oceanographic CTD profiler (<http://www.amloceanographic.com>) model Metrec-XL
9
10 147 equipped with a Turner Designs CYCLOPS-7 fluorometer (excitation 460 nm, emission, 620–715
11
12
13 148 nm). The absolute salinity (g kg^{-1}) and conservative temperature ($^{\circ}\text{C}$) were calculated from the
14
15 149 thermodynamic equation of seawater 2010 (TEOS-10) (IOC et al., 2010).
16
17
18 150 Water samples for quantitative analyses of microphytoplankton were collected in Niskin bottles
19
20 151 deployed every 2 m, from the surface to 20 m depth. The samples were immediately fixed with
21
22
23 152 acidic Lugol's solution (Lovegrove, 1960). During the February and March cruises, phytoplankton
24
25 153 samples (0–20 m water depth) were obtained by vertical net hauls (20- μm mesh), which provided
26
27
28 154 concentrated samples for marine toxins analyses. The samples were concentrated by filtration
29
30 155 through 1.2- μm GF/F filters (13-mm diameter) and stored in aqueous methanol (50%) for the
31
32 156 analysis of domoic acid (DA) and in 100% methanol for the analysis of lipophilic toxins.
33
34

35 157
36
37 158 ***2.4. Phytoplankton quantification***
38
39
40 159 Quantitative phytoplankton analyses were conducted in 10-mL unconcentrated samples fixed with
41
42 160 Lugol's acidic solution and left to sediment overnight. The phytoplankton were then analyzed
43
44
45 161 under an inverted microscope (Olympus CKX41) according to the method described in Utermöhl
46
47 162 (1958). The detection limit was 100 cells L^{-1} (i.e., one cell detected after examination of the entire
48
49
50 163 surface of the sedimentation chamber base-plate). Microphytoplankton were identified to the
51
52 164 species level when possible.
53
54
55
56
57
58
59
60
61
62
63
64
65

1
2
3
4
5
6
7
8
9
10
11
12
13
14
15
16
17
18
19
20
21
22
23
24
25
26
27
28
29
30
31
32
33
34
35
36
37
38
39
40
41
42
43
44
45
46
47
48
49
50
51
52
53
54
55
56
57
58
59
60
61
62
63
64
65

165 *Pseudo-nitzschia* species were separated into *P. delicatissima* and *P. seriata* complexes, based on
166 their length and valve width (Hasle, 1965). The samples were identified using an inverted
167 microscope (Zeiss, model Axio Vert. A1.).

169 **2.5. Electron microscopy of *Pseudo-nitzschia***

170 *Pseudo-nitzschia* cells in Lugol were treated to remove the organic matter from their frustules,
171 following the method described by Hasle (1978). Four mL of the cleaned sample was then filtered
172 through a gravity system using polycarbonate track-etched membranes filters Nucleopore (13-mm
173 diameter) (Whatman, UK). The filters were attached to stubs, sputter-coated with
174 platinum/palladium, and the cells trapped on the filters were observed using a Zeiss Auriga 60
175 microscope operated at 3 kV.

177 **2.6. Analysis of marine toxins**

178 **2.6.1. Toxin extraction**

179 Phytoplankton net samples were sonicated in an ultrasonic cell disruptor (Branson Sonic Power
180 450; Danbury, CT, USA). The sonicate was then clarified by centrifugation (20,000 g; 15 min) and
181 filtered through 0.20- μ m Clarinert nylon syringe filters (13 mm diameter) (Bonna-Agela
182 Technologies, Torrance, CA, USA). The filtrate was placed in amber vials and stored at -20°C for
183 subsequent use in analyses of domoic acid (DA) and of free okadaic acid (OA) and other lipophilic
184 toxins as described below. Samples for the analysis of esterified OA-group toxins were alkaline-
185 hydrolyzed following the standard procedure of the EU Reference Laboratory for Marine Biotoxins
186 (EURLMB, 2015), placed in amber vials and stored at -20°C .

1
2
3
4
5 188 **2.6.2. Detection and quantification of toxins**

6
7 189 Domoic acid was determined as previously described in Krock et al. (2008). In brief, the sample
8
9
10 190 was first analyzed in a hybrid triple quadrupole-linear ion trap mass spectrometer (API 4000
11
12 191 QTrap; Sciex, Darmstadt, Germany) coupled to a liquid chromatograph (LC1100, Agilent;
13
14 192 Waldbronn, Germany), after which the compounds of interest were separated by reversed-phase
15
16 193 chromatography on a C8 phase column (Hypersil BDS), 3 μm , 120 \AA (50 \times 2 mm), (Phenomenex,
17
18 194 Aschaffenburg, Germany) maintained at 20°C. The sample injection volume was 5 μL and the flow
19
20 195 rate 0.2 mL min^{-1} . Gradient elution was performed using aqueous eluent A and organic eluent B
21
22 196 (acetonitrile-water (95:5 v/v)), both containing 2.0 mM ammonium formate and 50 mM formic
23
24 197 acid. DA was detected in positive selected reaction monitoring mode using the mass transitions m/z
25
26 198 312/266 and 312/161. For the detection of OA, mass transitions of m/z 822/223, for DTX-1 m/z
27
28 199 836/237, for PTX-2 m/z 876/213, and for PTX-2sa m/z 894/213 were used. All toxins were
29
30 200 quantified by external calibration against standard solutions purchased from the certified reference
31
32 201 material (CRM) program of the ICB-NRC, Halifax, NS, Canada.
33
34
35
36
37
38
39
40
41

42 202
43 **3. Results**

44 203 **3.1. Regional climate conditions**

45 204
46 205 The regional-scale climate conditions over southern Chile during summer–fall 2018 are
47
48 206 summarized in the maps of bi-monthly rainfall anomalies shown in **Figure 2**. January and February,
49
50 207 at the height of summer, were markedly dry in the Los Lagos and Aysén regions (40–47°S), with
51
52 208 a rainfall deficit up to 70% (**Fig. 2A**). At Cisne Medio, the closest climatological station to
53
54 209 Magdalena Island (about 40 km inland), the accumulation during those 2 months was 151 mm,
55
56
57
58 210 well below the mean accumulation of 281 mm, with February 2018 as the driest month (50%
59
60
61
62
63
64
65

1
2
3
4
5 211 deficit). The low precipitation was accompanied by above average solar radiation reaching the
6
7
8 212 surface during most of the summer (not shown). During early fall, precipitation across much of
9
10 213 southern and austral Chile (38–55°S) was well above average, with rainfall anomalies increasing
11
12
13 214 precipitation above the mean by 60–80% over central Patagonia (Fig. 1B). At Cisne Medio, nearly
14
15 215 500 mm of rainfall accumulated during March–April 2018, higher than the mean of 360 mm.
16
17 216 The marked contrast between the dry summer and wet fall was consistent with the disparate number
18
19
20 217 of synoptic-scale disturbances that reached southern South America during that period and well
21
22 218 captured by the meteorological time series over Magdalena Island from ERA5. The precipitation
23
24
25 219 series (Fig. 3A) revealed few and minor rainfall events during January–February, with the dry-wet
26
27 220 transition occurring very rapidly, around the first week of March, and frequent (1–2 per week) and
28
29
30 221 major events during March–April (Fig. 3A). Most of these rainfall events during March–April 2018
31
32 222 were associated with ARs, in sharp contrast to the lack of ARs in the preceding two months.
33
34
35 223 During the study period, the first AR reached the region on 7–8 March 2018 (Figure 3D). The moist
36
37 224 air filament, largely concentrated in the first 2–3 km above sea level (asl), was driven by intense
38
39 225 WNW winds that also signaled a low-level dome of cold air progressing from south to north. These
40
41
42 226 two features and the resulting copious precipitation are commonly associated with landfalling ARs
43
44 227 and were also evident in the time series of the zonal wind and air temperature at 850 hPa (~1500
45
46
47 228 m asl) over Magdalena Island (Fig. 3B-C). Early March thus marked a shift in the regional
48
49 229 meteorological conditions, from an exceptionally dry, sunny, warm and calm (weak westerlies)
50
51
52 230 summer to an anomalous wet, cloudy, cold and windy (strong westerlies) fall. The mechanism and
53
54 231 impact of these dramatic changes are discussed in the next sections.
55
56
57 232

59 233 ***3.2. Hydrographic conditions***

1
2
3
4
5 234 The temporal evolution of the meteorological conditions that occurred in summer and early
6
7
8 235 autumn 2018 were also apparent in the water column structure (Fig. 4). Early summer (January–
9
10 236 February) was characterized by strongly thermo-haline-stratified conditions with a typical two-
11
12
13 237 layered structure (Fig. 4A, B). A maximum temperature gradient of $5.3^{\circ}\text{C } 10 \text{ m}^{-1}$ and a salinity
14
15 238 gradient of $17.2 \text{ } 10 \text{ m}^{-1}$ were detected in January. Towards the end of summer–beginning of
16
17
18 239 autumn, the water column became more homogeneous, with temperature and salinity gradients of
19
20 240 $0.4^{\circ}\text{C } 10 \text{ m}^{-1}$ and $7.0 \text{ } 10 \text{ m}^{-1}$ in March. In general, surface (0–2 m) temperatures and salinities
21
22
23 241 ranged from 18.2 to 10.6°C and from 11.9 to 22.9 g kg^{-1} , respectively. The minimum temperature,
24
25 242 reached in April, was probably associated with the start of the thermal inversion process (Fig. 4A).
26
27 243 Strong stratification in the upper 10 m was accompanied by a Brunt-Väisälä frequency that in
28
29
30 244 January reached a maximum ($60\text{--}100 \text{ cycles h}^{-1}$) in the inter-phase between estuarine fresh water
31
32 245 (salinities $11\text{--}21 \text{ g kg}^{-1}$) and estuarine salty water ($21\text{--}31 \text{ g kg}^{-1}$) (Fig. 4C). High levels of
33
34
35 246 dissolved oxygen ($>6 \text{ ml L}^{-1}$; $>90\%$ saturation) and a high pH (>8) were likewise detected in this
36
37 247 upper layer (Fig. 4D, E). Chlorophyll *a* (fluorescence) levels were highest in a layer extending
38
39
40 248 from the surface to 10 m depth, with a maximum of $15.2 \text{ } \mu\text{g L}^{-1}$ recorded on April 23, 2018 at 4
41
42 249 m depth and forming an intense thin layer between 2 and 6 m depth (Fig. 4F).
43

44 250
45

47 251 ***3.3. Phytoplankton community succession and marine biotoxins***

48
49 252 The phytoplankton analysis revealed a phytoplankton community dominated by diatoms ($>96\%$)
50
51
52 253 at the beginning of the summer (Fig. 5). On January 17, 2018, the phytoplankton community
53
54 254 reached a maximum cell density of $450 \times 10^3 \text{ cells L}^{-1}$ and was dominated by the diatom *Pseudo-*
55
56 255 *nitzschia delicatissima* complex (96.9%), associated with a strong thermo-haline stratification
57
58
59 256 (Figs. 5A–C). One month later, on February 16, 2018, the structure of phytoplankton community
60
61
62
63
64
65

1
2
3
4
5 257 underwent a significant change, with a maximum cell density of 109×10^3 cells L^{-1} and a clear
6
7
8 258 dominance of the dinoflagellate *D. acuta* (96.3%). Fine-scale vertical resolution sampling showed
9
10 259 an intense thin layer made up of cells of this species, with a maximum density of 105.4×10^3 cells
11
12
13 260 L^{-1} , located at 6 m depth. The detection coincided with maximum temperature and salinity
14
15 261 gradients ($0.49^\circ C m^{-1}$ and $1.49 g kg^{-1} m^{-1}$) (Fig. 5D–F). The analysis of net tow extracts by liquid
16
17 262 chromatography coupled to mass spectrometry (LC-MS) revealed the presence of diarrhetic
18
19
20 263 shellfish toxins (OA and DTX-1) and pectenotoxins (PTX-2, PTX-2sa, and PTX-2sa isomer) in
21
22 264 different proportions (Fig. 6). The highest concentrations were those of DTX-1 and OA (231 and
23
24
25 265 $72 ng NT^{-1}$, respectively) followed by PTX-2 ($20 ng NT^{-1}$). On March 12, the phytoplankton
26
27 266 composition changed again, with the resumption of a clear dominance of diatoms (>99%) that
28
29
30 267 coincided with the arrival of an AR (Fig. 3). Thus, the intense February bloom of *D. acuta* was
31
32 268 significantly reduced (max. 2.5×10^3 cells L^{-1}), as it gave way to an intense bloom of *P.*
33
34
35 269 *delicatissima* complex, with a maximum cell density of 1.560×10^3 cells L^{-1} at 2 m. A second
36
37 270 maximum of 1.300×10^3 cells L^{-1} was detected at 16 m depth (Fig. 5G–I). LC-MS/MS analysis of
38
39
40 271 net tow extracts prepared from the *Pseudo-nitzschia* bloom showed the presence of DA, at a
41
42 272 concentration of $45 ng NT^{-1}$, as well as DTX-1, OA, and PTX-2, albeit at lower concentrations of
43
44 273 28 and $10 ng NT^{-1}$, respectively (Fig. 6). On April 23, the density of the *P. delicatissima* complex
45
46
47 274 bloom increased. The cells formed a well-defined thin layer between 2 and 6 m (Fig. 5J–L), with
48
49 275 a maximum of $3,382 \times 10^3$ cells L^{-1} at 4 m, that followed the vertical structure of the chlorophyll
50
51
52 276 *a* concentration, which reached a maximum of $15.4 \mu g L^{-1}$ at the same depth (Fig. 5J, K). In March,
53
54 277 the phytoplankton community was still dominated by *P. delicatissima* complex (>99% at the thin
55
56
57 278 layer depths; Fig. 5L).

1
2
3
4
5
6
7
8
9
10
11
12
13
14
15
16
17
18
19
20
21
22
23
24
25
26
27
28
29
30
31
32
33
34
35
36
37
38
39
40
41
42
43
44
45
46
47
48
49
50
51
52
53
54
55
56
57
58
59
60
61
62
63
64
65

279
280
281
282
283
284
285
286
287
288
289
290
291
292
293
294
295
296
297
298
299
300

3.4. Taxonomic identification of *Pseudo-nitzschia*

Light microscopy (LM) of the samples confirmed the dominance of cells from *P. delicatissima* complex. The length and width of the cells ranged from 66 to 86 μm ($77.7\pm 3.9 \mu\text{m}$) and from 1.1 to 2 μm ($1.5\pm 0.3 \mu\text{m}$), respectively. Scanning electron microscopy analysis revealed the presence of *P. calliantha* (Fig. 7). The cells were linear in valve view (Fig. 7A), with an apical axis of 66–80 μm , a transapical axis of 1.3–1.8 μm (Fig. 7B, C) and a large central nodule (Fig. 7D, E). The fibulae and striae (19–22 and 37–39 per 10 μm , respectively) were regularly spaced. The striae were formed by one row of round poroids with a density 4–6 per 1 μm . The hymen of the poroids was perforated to form 6–12 sectors (Table 1).

4. Discussion

The spatial and temporal distributions of phytoplankton assemblages in estuarine and shallow coastal water are closely linked to atmospheric and hydrographic conditions. In the latter, nutrient availability and turbulence play fundamental roles in phytoplanktonic community structure (Margalef, 1978; Margalef et al., 1979; Smayda and Reynolds, 2001). Although some aspects of phytoplankton succession in the study area are relatively well known, mainly those related to turbulence-induced transitions between toxic dinoflagellates and diatoms, our results substantially expand current knowledge about the relationships between toxic phytoplankton successions and atmospheric-hydrographic parameters, as they showed that mid-latitude storms and ARs are important factors triggering population shifts in phytoplankton. We also present the first report of a toxic species of *Pseudo-nitzschia* in NW Patagonia. The information provided by our study will

1
2
3
4
5
6
7
8
9
10
11
12
13
14
15
16
17
18
19
20
21
22
23
24
25
26
27
28
29
30
31
32
33
34
35
36
37
38
39
40
41
42
43
44
45
46
47
48
49
50
51
52
53
54
55
56
57
58
59
60
61
62
63
64
65

301 help in evaluating the threats to shellfish farming posed by HABs and will improve predictions of
302 toxic events, by incorporating environmental parameters.

303
304 **4.1. Broad-scale climate forcing**

305 The warmest and driest conditions in northern Patagonia occur at the height of the austral summer,
306 and the coldest wettest conditions in winter. This climate transition was particularly marked in
307 2018 because of an anomalous dry and warm summer that was followed by an equally anomalous
308 wet and cold fall. The shift in the regional climate took place in early March, fostered by the arrival
309 of several ARs, each accompanied by large amounts of precipitation, cold air and strong westerly
310 winds (Fig. 3A–C).

311 The contrasting conditions between summer and fall are regional manifestations of large-scale
312 circulation changes, illustrated by the sea-level pressure anomalies in the inset maps of Figure 2A,
313 B. During January–February, a persistent band of high pressure extended from the Pacific to the
314 Atlantic at about 45°S, hindering the passage of mid-latitude weather systems and weakening the
315 westerlies against the southern Andes, resulting in a rainfall deficit. On a hemispheric scale,
316 negative anomalies prevailed at high latitudes and positive anomalies at mid-latitudes, i.e., the
317 fingerprint of the positive phase of the Southern Annular Mode (SAM, Thompson and Wallace,
318 2000), whose index (Marshall, 2003) reached +1.1 hPa in the summer of 2018 (Fig. 2C). This
319 highly positive value was in part due to the tendency of the SAM to maintain the positive polarity
320 that has prevailed during the last three to four decades (Fogt and Marshall, 2020; Thompson and
321 Wallace, 2000). The positive SAM trend in summer has been linked to the anthropogenically forced
322 increase in greenhouse gas concentrations in the troposphere and to the decrease in the ozone layer
323 in the polar stratosphere (Arblaster and Meehl, 2006; Gillett et al., 2013); it also explains much of

1
2
3
4
5 324 the contemporaneous drying in northern Patagonia during summer (Garreaud et al., 2013; Gillett
6
7
8 325 et al., 2006). In early fall, the large-scale pattern reversed, with positive pressure anomalies
9
10 326 prevailing over Antarctica and negative pressure anomalies across the mid-latitudes of the Southern
11
12
13 327 Hemisphere, causing a steep drop of the SAM index to -0.6 hPa (Fig. 2C). A change in SAM
14
15 328 polarity between January–February and March–April is not uncommon, given the high variability
16
17
18 329 and low autocorrelation of the SAM at monthly time scales as well as the weaker trend in the SAM
19
20 330 in fall (Fogt and Marshall, 2020). Within the negative SAM pattern during March–April 2018, a
21
22
23 331 cyclonic anomaly developed near the southern tip of the continent (Fig. 2B), increasing the strength
24
25 332 of the westerlies at mid-latitudes that drive ARs toward southern South America, resulting in excess
26
27 333 precipitation across Patagonia.
28
29
30 334

31 32 335 ***4.2. Toxic phytoplankton succession and hydroclimatic modulation*** 33

34
35 336 According to Margalef’s mandala model (Margalef, 1978), turbulent environments are associated
36
37 337 with diatoms and stable conditions with dinoflagellates. Diatoms tend to dominate during periods
38
39
40 338 of mixing and high nutrient concentrations, because of the numerous advantages conferred by their
41
42 339 higher growth rates, higher photosynthetic rates and improved ability to compete for nitrogen at
43
44 340 low cell densities (Estrada et al., 1987; Estrada and Berdalet, 1997). Conversely, dinoflagellates
45
46
47 341 prevail in more stable, oligotrophic systems, because turbulence has harmful effects on their
48
49 342 morphology (Berdalet and Estrada, 1995), cleavage rate (Thomas and Gibson, 1990a, b; Thomas
50
51
52 343 et al., 1995) and growth (Gibson and Thomas, 1995). Thermo-haline stratification of the water
53
54 344 column facilitates the accumulation of dinoflagellates at more stable depths, such as the pycnocline
55
56 345 (Díaz et al., 2021).
57
58
59
60
61
62
63
64
65

1
2
3
4
5 346 Based on the models proposed by Margalef (1978) and Reynolds (2002), Alves de Souza *et al.*
6
7
8 347 (2008) suggested that the distribution and abundance of phytoplankton assemblages in southern
9
10 348 Chile are mostly determined by the stability of the water column and the nutrient concentration.
11
12
13 349 The present work documented the succession of toxic phytoplankton communities in Puyuhuapi
14
15 350 Fjord during early 2018. *D. acuta* (producer of lipophilic toxins) was dominant in summer
16
17
18 351 (January–February), as it thrives in a highly stratified water column, while *Pseudo-nitzschia*
19
20 352 *calliantha* (producer of hydrophilic DA) bloomed and was dominant in March–April, when the
21
22
23 353 water column became mixed. However, our study also identified forces acting outside of
24
25 354 Margalef’s mandala, as the change in water column stability could be directly linked to regional
26
27
28 355 meteorological conditions as the driver. Indeed, the prominent stratification of the water column in
29
30 356 summer 2018 was consistent with the extremely dry, sunny, warm, calm (weak winds) conditions
31
32 357 that prevailed during those months, which in turn were caused by anticyclonic anomalies over the
33
34
35 358 southern tip of South America and the positive phase of SAM. Likewise, the mixed water column
36
37 359 during March–April was coincident with the rainy, cold, windy conditions of early fall, in
38
39
40 360 connection with a reversed large-scale atmospheric pattern (negative phase of SAM). The
41
42 361 hydrographic cross-sections (Fig. 4) showed a smooth transition, although the monthly-scale
43
44 362 sampling schedule should be noted. By contrast, the sub-daily meteorological data revealed a
45
46
47 363 sharper transition between summer and fall conditions during the first half of March (Fig. 3A–C).
48
49 364 Of particular relevance was the arrival of several ARs in northern Patagonia, with the first strong
50
51
52 365 AR reaching the study area during 6–8 March 2020 (Fig. 3D). In addition to bringing copious
53
54 366 rainfall and cold air, the ARs were accompanied by strong winds blowing from the northwest. As
55
56
57 367 Magdalena Sound is oriented in the west-east direction and located within a tall, narrow mountain
58
59 368 canyon (Fig. 1C), the large-scale northwest winds during the ARs were likely amplified over the
60
61
62
63
64
65

1
2
3
4
5 369 sound. The resulting strong surface wind stress may have been the main driver of the water column
6
7
8 370 mixing that ultimately caused the toxic phytoplankton succession reported herein. However, high-
9
10 371 resolution coupled ocean-atmosphere simulations need to be carried out to confirm the role of this
11
12
13 372 abiotic component in the succession.

14
15 373

17 374 **4.3. *Pseudo-nitzschia calliantha* and the potential impact of DA**

20 375 The few taxonomic identifications of *Pseudo-nitzschia* species in the study area include those in
21
22 376 comprehensive studies by Hasle (1972) and Rivera (1985). However, *Pseudo-nitzschia* includes
23
24
25 377 cryptic species that cannot be readily identified by light microscopy, such that in recent
26
27 378 oceanographic studies the specimens were categorized within two main complexes: *Pseudo-*
28
29
30 379 *nitzschia seriata* and *Pseudo-nitzschia delicatissima* (Alves de Souza et al., 2008; Cassis et al.,
31
32 380 2002; Montero et al., 2017; Pizarro et al., 2018). Among the toxins produced by *Pseudo-nitzschia*
33
34
35 381 are DA, with its first detection in southern Chile occurring in clams from Chiloé Island during the
36
37 382 austral summer of 1997, in association with the presence of *P. australis* (Suárez-Isla et al., 2002).
38
39 383 In 2000, a major outbreak of amnesic shellfish poisoning, which is caused by DA, in the same area
40
41
42 384 resulted in the closure of a local natural mussel bank for more than a month, because the mussel
43
44 385 DA content exceeded the regulatory limit (20 mg kg⁻¹) (Suárez-Isla et al., 2002). Again, the
45
46
47 386 responsible species was likely *P. australis*, although a morphologically similar cell belonging to
48
49 387 the *Pseudo-nitzschia delicatissima* complex was also present in some areas (Díaz et al., 2019).

51 388 Given that *Pseudo-nitzschia* is responsible for nearly all toxic algal bloom events in upwelling
52
53
54 389 regions around the world and the serious threat it poses to mariculture and wild fauna, the need for
55
56
57 390 knowledge of the conditions that promote these events is clear (Torres-Palenzuela et al., 2019).
58
59 391 However, as noted above, a precise classification of the species comprising *Pseudo-nitzschia* by

1
2
3
4
5 392 light microscopy is difficult, such that most reports on *Pseudo-nitzschia* blooms do not include a
6
7
8 393 precise identification. Specifically, *P. calliantha* is found worldwide but was previously described
9
10 394 as toxic and non-toxic (see Bates et al., 2018 and references therein; Lelong et al., 2012; Trainer et
11
12
13 395 al., 2012), although the presence of this species in Chilean coastal waters and its production of DA
14
15 396 were previously described by (Álvarez et al., 2009). In addition to being the first report of toxic *P.*
16
17
18 397 *calliantha* in NW Patagonia, our study establishes a relationship between the presence of this
19
20 398 species and the occurrence of ARs. Thus, in addition to important knowledge on the composition
21
22
23 399 of the toxic phytoplankton community in the PFS, it provides insights into the general factors
24
25 400 governing toxic phytoplankton successions and potential sources of DA in upwelling systems
26
27 401 around the world.
28
29

30 402
31
32 403 ***4.4. Lipophilic toxins, biotransformation and its potential negative impacts on the early stages***
33
34
35 404 ***of shellfish development***
36

37 405 In Chilean Patagonia, *D. acuta* is the most harmful of the lipophilic toxin producers and its blooms
38
39 406 are always associated with the occurrence of OA, DTX1 and PTXs, detected in shellfish and
40
41
42 407 plankton samples (reviewed by Díaz et al., 2022a). Profiles of plankton samples from Puyuhuapi
43
44 408 Fjord are similar to those determined in previous studies of the fjord (Baldich et al., 2023; Baldrich
45
46
47 409 et al., 2021; Díaz et al., 2021). However, as PTX2 is the only pectenotoxin found in *D. acuta*, the
48
49 410 detection of PTX-2sa, and PTX-2sa isomers suggests that they are produced via the
50
51
52 411 biotransformation of PTX2 by species of higher trophic levels, such as zooplankton (Blanco et al.,
53
54 412 2007).
55

56 413 While the conditions leading to toxic bloom events by *Dinophysis* and *Pseudo-nitzschia* in the PFS
57
58
59 414 are not uncommon, the consequences for fisheries, aquaculture and human health have been
60
61
62
63
64
65

1
2
3
4
5 415 scarcely evaluated. The main reason is that most of the toxic outbreaks thus far have been caused
6
7
8 416 by *Alexandrium catenella*, responsible for the accumulation of paralytic shellfish toxins (PST) in
9
10 417 natural banks of shellfish (Díaz et al., 2022b; Molinet et al., 2010) and the considerable socio-
11
12
13 418 economic impacts of these toxic events. In Chile, the potential negative impacts of *Dinophysis*
14
15 419 species and/or their associated toxins on marine invertebrates, including shellfish species, have
16
17
18 420 received little attention. However, the exposure of mussels to OA reduces protein phosphatase
19
20 421 activity and larval viability in *Mytilus edulis* (De Rijcke et al., 2015) whereas neither the activity
21
22
23 422 nor the viability of the eastern oyster *Crassostrea virginica* is affected (Pease et al., 2022). In
24
25 423 Pacific oysters (*Magallana gigas*) exposed to PTX2, fertilization success is reduced and larval
26
27
28 424 mortality rates are increased (Gaillard et al., 2020). Similarly, in *C. virginica* larvae, PTX2
29
30 425 exposure induces immobilization and rapid mortality (nearly 50%) (Pease et al., 2022).
31
32 426 Finally, further research into the interplay of atmospheric and hydrographic conditions in the PFS
33
34
35 427 is needed in order to understand their combined impact on plankton communities in this semi-
36
37 428 enclosed environment. A better understanding of plankton dynamics and the negative effects of
38
39
40 429 lipophilic toxins on bivalve species, especially juvenile stages, will lay the basis for more accurate
41
42 430 assessments of HAB-related risks and the more effective management of seafood aquaculture in
43
44 431 this region.

45
46
47 432
48
49 433 **Acknowledgements**
50
51
52 434 This study was funded by projects REDI170575 and REDES170101 from the International
53
54 435 Cooperation Programme of ANID and partly supported by the Helmholtz-Gemeinschaft Deutscher
55
56
57 436 Forschungszentren through the research program “Changing Earth - Sustaining our Future” of the
58
59 437 Alfred Wegener Institut (AWI)-Helmholtz Zentrum für Polar- und Meeresforschung. The authors
60
61
62
63
64
65

1
2
3
4
5 438 thank Annegret Müller (AWI) for sample processing and Thomas Max (AWI) for LC-MS/MS
6
7
8 439 measurements. P.A. Díaz was funded by FONDECYT-ANID 11170682 and by the Centre for
9
10 440 Biotechnology and Bioengineering (CeBiB) (PIA project FB0001, ANID, Chile). G. Álvarez was
11
12
13 441 funded by FONDEF/CONICYT 2017, IT17F10002. Iván Perez-Santos was funded by COPAS
14
15 442 Sur-Austral (ANID AFB170006), COPAS COASTAL (ANID FB210021), CIEP R20F002, and
16
17
18 443 FONDECYT 1211037. Rosa I. Figueroa was funded by a national project from the Spanish
19
20 444 Ministry of Science and Innovation and the European Community, European Regional
21
22 445 Development Fund (ERDF; Project BIOTOX PID2021-1256430B-C22).
23
24
25 446

27 447 **References**

29
30 448 Álvarez, G., Díaz, P.A., Godoy, M., Araya, M., Ganuza, I., Pino, R., Álvarez, F., Rengel, J.,
31
32 449 Hernández, C., Uribe, E., Blanco, J., 2019. Paralytic Shellfish Toxins in *Mesodesma*
33
34 450 *donacium* during an exceptional bloom of *Alexandrium catenella* associated to an intense
35
36 451 mass mortality. *Toxins* 11, 188.
37
38
39 452 Álvarez, G., Uribe, E., Quijano-Scheggia, S., López-Rivera, A., Mariño, C., Blanco, J., Gonzalo,
40
41
42 453 A., Blanco, J., Marin, C., 2009. Domoic acid production by *Pseudo-nitzschia australis* and
43
44 454 *Pseudo-nitzschia calliantha* isolated from North Chile. *Harmful Algae* 8, 938-945.
45
46
47 455 Álvarez-Garreton, C., Mendoza, P.A., Boisier, J.P., Addor, N., Galleguillos, M., Zambrano-
48
49 456 Bigiarini, M., Lara, A., Puelma, C., Cortes, G., Garreaud, R., McPhee, J., Ayala, A., 2018.
50
51 457 The CAMELS-CL dataset: catchment attributes and meteorology for large sample studies
52
53
54 458 – Chile dataset. *Hydrology and Earth System Sciences* 22.
55
56
57
58
59
60
61
62
63
64
65

- 1
2
3
4
5 459 Alves de Souza, C., González, M.T., Iriarte, J.L., 2008. Functional groups in marine phytoplankton
6
7
8 460 assemblages dominated by diatoms in fjords of southern Chile. *J. Plankton Res.* 30, 1233-
9
10 461 1243.
- 11
12 462 Alves de Souza, C., Varela, D., Contreras, C., de la Iglesia, P., Fernández, P., Hipp, B., Hernández,
13
14
15 463 C., Riobó, P., Reguera, B., Franco, J.M., Diogene, J., García, C., Lagos, N., 2014. Seasonal
16
17 464 variability of *Dinophysis* spp. and *Protoceratium reticulatum* associated to lipophilic
18
19 465 shellfish toxins in a strongly stratified Chilean fjord. *Deep Sea Res. II* 101, 152-162.
- 20
21
22 466 Arblaster, J.M., Meehl, G., 2006. Contributions of external forcings to Southern Annular Mode
23
24
25 467 trends. *J. Climate* 19, 2896–2905.
- 26
27 468 Baldich, A.M., Díaz, P.A., Álvarez, G., Pérez-Santos, I., Schwerter, C., Díaz, M., Araya, M.,
28
29
30 469 Nieves, M.G., Rodríguez-Villegas, C., Barrera, F., Fernández-Pena, C., Arenas-Uribe, S.,
31
32 470 Navarro, P., Reguera, B., 2023. *Dinophysis acuminata* or *Dinophysis acuta*: What Makes
33
34
35 471 the Difference in Highly Stratified Fjords? *Mar. Drugs* 21, 64.
- 36
37 472 Baldrich, A., Pérez-Santos, I., Álvarez, G., Reguera, B., Fernández-Pena, C., Rodríguez-Villegas,
38
39
40 473 C., Araya, M., Álvarez, F., Barrera, F., Karasiewicz, S., Díaz, P.A., 2021. Niche
41
42 474 differentiation of *Dinophysis acuta* and *D. acuminata* in a stratified fjord. *Harmful Algae*
43
44 475 103, 102010.
- 45
46
47 476 Bates, S.S., Hubbard, K.A., Lundholm, N., Montresor, M., Leaw, C.P., 2018. *Pseudo-nitzschia*,
48
49 477 *Nitzschia*, and domoic acid: New research since 2011. *Harmful Algae* 79, 3-43.
- 50
51
52 478 Berdalet, E., Estrada, M., 1995. Effects of turbulence on several phytoplankton species, in:
53
54 479 Smayda, T.J., Shimizu, Y. (Eds.), *Toxic Phytoplankton Blooms in the Sea*, pp. 737–740.
- 55
56
57
58
59
60
61
62
63
64
65

- 1
2
3
4
5 480 Blanco, J., Álvarez, G., Uribe, E., 2007. Identification of pectenotoxins in plankton, filter feeders,
6
7
8 481 and isolated cells of a *Dinophysis acuminata* with an atypical toxin profile, from Chile.
9
10 482 Toxicon 49, 710-716.
- 11
12 483 Cassis, D., Muñoz, P., Avaria, S., 2002. Variación temporal del fitoplancton entre 1993 y 1998 en
14
15 484 una estación fija del seno Aysén, Chile (45°26'S 73°00'W). Rev. Biol. Mar. Ocenog. 37, 43-
16
17 485 65.
- 18
19 486 Contreras, H.R., García, C., 2019. Inter-species variability of okadaic acid group toxicity in relation
21
22 487 to the content of fatty acids detected in different marine vectors. Food Addit. Contam. Part
23
24 488 A 36, 464-482.
- 25
26 489 De Rijcke, M., Vandegehuchte, M., Vanden Bussche, J., Nevejan, N., Vanhaecke, L., De
27
28 490 Schamphelaere, K., Janssen, C., 2015. Common European harmful algal blooms affect the
29
30 491 viability and innate immune responses of *Mytilus edulis* larvae. Fish & Shellfish
31
32 492 Immunology 47, 175-181.
- 33
34 493 Díaz, P.A., Álvarez, A., Varela, D., Pérez-Santos, I., Díaz, M., Molinet, C., Seguel, M., Aguilera-
35
36 494 Belmonte, A., Guzmán, L., Uribe, E., Rengel, J., Hernández, C., Segura, C., Figueroa, R.I.,
37
38 495 2019. Impacts of harmful algal blooms on the aquaculture industry: Chile as a case study.
39
40 496 Perspect. Phycol. 6, 39-50.
- 41
42 497 Díaz, P.A., Álvarez, G., Pizarro, G., Blanco, J., Reguera, B., 2022a. Lipophilic toxins in Chile:
43
44 498 History, producers and impacts. Mar. Drugs 20, 122.
- 45
46 499 Díaz, P.A., Molinet, C., Seguel, M., Díaz, M., Labra, G., Figueroa, R., 2014. Coupling planktonic
50
51 500 and benthic shifts during a bloom of *Alexandrium catenella* in southern Chile: Implications
52
53 501 for bloom dynamics and recurrence. Harmful Algae 40, 9-22.
- 54
55
56
57
58
59
60
61
62
63
64
65

1
2
3
4
5 502 Díaz, P.A., Molinet, C., Seguel, M., Niklitschek, E.J., Díaz, M., Álvarez, G., Pérez-Santos, I.,
6
7
8 503 Varela, D., Guzmán, L., Rodríguez-Villegas, C., Figueroa, R.I., 2022b. Modelling the
9
10 504 spatial and temporal dynamics of paralytic shellfish toxins (PST) at different scales:
11
12
13 505 Implications for research and management. *Toxins* 14, 786.
14
15 506 Díaz, P.A., Pérez-Santos, I., Álvarez, G., Garreaud, R., Pinilla, E., Díaz, M., Sandoval, A., Araya,
16
17 507 M., Álvarez, F., Rengel, J., Montero, P., Pizarro, G., López, L., Iriarte, L., Igor, G., Reguera,
18
19
20 508 B., 2021. Multiscale physical background to an exceptional harmful algal bloom of
21
22 509 *Dinophysis acuta* in a fjord system. *Sci. Total Environ.* 773, 145621.
23
24
25 510 Díaz, P.A., Pérez-Santos, I., Basti, L., Garreaud, R., Pinilla, E., Barrera, F., Tello, A., Schwerter,
26
27 511 C., Arenas-Uribe, S., Soto-Riquelme, C., Navarro, P., Díaz, M., Álvarez, G., Linford, P.,
28
29
30 512 Altamirano, R., Mancilla-Gutiérrez, G., Rodríguez-Villegas, C., Figueroa, R.I., 2023. How
31
32 513 local and climate change drivers shaped the formation, dynamics and potential recurrence
33
34
35 514 of a massive fish-killer microalgal bloom in Patagonian fjord. *Sci. Total Environ.* 865,
36
37 515 161288.
38
39 516 Estrada, M., Alcaraz, M., Masarré, C., 1987. Effects of turbulence on the composition of
40
41
42 517 phytoplankton assemblages in marine microcosms. *Mar. Ecol. Prog. Ser.* 38, 267-281.
43
44 518 Estrada, M., Berdalet, E., 1997. Phytoplankton in a turbulent world. *Scientia Marina* 61, 125-140.
45
46
47 519 Fogt, R.L., Marshall, G.J., 2020. The Southern Annular Mode: Variability, trends, and climate
48
49 520 impacts across the Southern Hemisphere. *WIREs Clim. Change* 11, e652.
50
51
52 521 Försterra, G., 2009. Ecological and biogeographical aspects of the Chilean Fjord region, in:
53
54 522 Haussermann, V., Försterra, G. (Eds.), *Marine Benthic Fauna of Chilean Patagonia. Nature*
55
56 523 *in Focus*, Puerto Montt, Chile, pp. 61–76.
57
58
59
60
61
62
63
64
65

1
2
3
4
5 524 Gaillard, S., Le Goïc, N., Malo, F., Boulais, M., Fabioux, C., Zaccagnini, L., Carpentier, L., Sibat,
6
7
8 525 M., Réveillon, D., Séchet, V., Hess, P., Hégaret, H., 2020. Cultures of *Dinophysis sacculus*,
9
10 526 *D. acuminata* and pectenotoxin 2 affect gametes and fertilization success of the Pacific
11
12
13 527 oyster, *Crassostrea gigas*. Environ. Pollut. 265, 114840.
14
15 528 García, C., Rodríguez-Unda, N., Contreras, C., Barriga, A., Lagos, N., 2012. Lipophilic toxin
16
17 529 profiles detected in farmed and benthic mussels populations from the most relevant
18
19
20 530 production zones in Southern Chile. Food Addit. Contam. Part A 29, 1011-1020.
21
22 531 Garreaud, R., Lopez, P., Minvielle, M., Rojas, M., 2013. Large-scale control on the Patagonian
23
24
25 532 climate. J. Climate 26, 215-230.
26
27 533 GEOHAB, 2010. Global Ecology and Oceanography of Harmful Algal Blooms, GEOHAB Core
28
29
30 534 Research Project: HABs in Fjords and Coastal Embayments. A. Cembella, L. Guzmán, S.
31
32 535 Roy, J. Diogène (Eds.), IOC and SCOR, Paris, France and Newark, Delaware USA, 57 pp.
33
34
35 536 Gibson, C.H., Thomas, W.H., 1995. Effects of turbulence intermittency on growth inhibition of a
36
37 537 red tide dinoflagellate, *Gonyaulax polyedra* Stein. J. Geophys. Res. 100, 24841-24846.
38
39 538 Gillett, N.P., Arora, V.K., Matthews, D., Allen, M.R., 2013. Constraining the ratio of global
40
41
42 539 warming to cumulative CO2 emissions using CMIP5 simulations. J. Climate 26, 844–6858.
43
44 540 Gillett, N.P., Kell, T.D., Jones, P.D., 2006. Regional climate impacts of the Southern Annular
45
46
47 541 Mode. Geophys. Res. Lett. 33, L23704.
48
49 542 Guzmán, L., Pacheco, H., Pizarro, G., Alárcon, C., 2002. *Alexandrium catenella* y veneno
50
51 543 paralizante de los mariscos en Chile, in: Sar, E.A., Ferrario, M.E., Reguera, B. (Eds.),
52
53
54 544 Floraciones Algales Nocivas en el Cono Sur Americano. Instituto Español de Oceanografía,
55
56 545 Madrid, pp. 235-255.
57
58
59
60
61
62
63
64
65

- 1
2
3
4
5 546 Hasle, G.R., 1965. *Nitzschia* and *Fragilariopsis* species studied in the light and electron
6
7
8 547 microscopes. II. The group *Pseudonitzschia*. Skr. Norske Vidensk-Akad. I. Mat.-Nat. Kl.
9
10 548 Ny Series 18, 1-45.
11
12
13 549 Hasle, G.R., 1972. The distribution of *Nitzschia seriata* and allied species. Nova Hedwigia, Beith
14
15 550 39, 171-190.
16
17
18 551 Hasle, G.R., 1978. The Inverted-Microscope Methods, in: Sournia, A. (Ed.), Phytoplankton
19
20 552 Manual. United Nations Educational, Scientific, and Cultural Organization, Paris, pp. 88-
21
22 553 96.
23
24
25 554 Haury, L.R., McGowan, J.A., Wiebe, P.H., 1978. Patterns and processes in the time-space scales
26
27 555 of plankton distribution, in: Steele, J.H. (Ed.), Spatial Pattern in Plankton Communities.
28
29
30 556 Springer Science, Plenum, New York, pp. 277-327.
31
32 557 Häussermann, V., Gutstein, C.S., Bedington, M., Cassis, D., Olavarria, C., Dale, A.C., Valenzuela-
33
34 558 Toro, A.M., Perez-Alvarez, M.J., Sepúlveda, H.H., McConnell, K.M., Horwitz, F.E.,
35
36
37 559 Försterra, G., 2017. Largest baleen whale mass mortality during strong El Niño event is
38
39 560 likely related to harmful toxic algal bloom. PeerJ 5, e3123
40
41
42 561 <https://doi.org/3110.7717/peerj.3123>.
43
44 562 Hersbach, H., Bell, B., Berrisford, P., Hirahara, S., Horányi, S., Muñoz-Sabater, J., Nicolas, J.,
45
46
47 563 Peubey, C., Radu, R., Schepers, D., Simmons, A., Soci, C., Abdalla, S., Abellan, X.,
48
49 564 Balsamo, G., Bechtold, P., Biavati, G., Bidlot, J., Bonavita, M., De Chiara, G., Dahlgren,
50
51
52 565 P., Dee, D., Diamantakis, M., Dragani, R., Flemming, J., Forbes, R., Fuentes, M., Geer, A.,
53
54 566 Haimberger, L., Healy, S., Hogan, R.J., Hólm, E., Janisková, M., Keeley, S., Laloyaux, P.,
55
56
57 567 Lopez, P., Lupu, C., Radnoti, G., de Rosnay, P., Rozum, I., Vamborg, F., Villaume, S.,
58
59
60
61
62
63
64
65

1
2
3
4
5 568 Thépaut, J.-N., 2020. The ERA5 global reanalysis. Quarterly Journal of the Royal
6
7
8 569 Meteorological Society 146, 1999-2049.
9
10 570 IOC, SCOR, IAPSO, 2010. The international thermodynamic equation of seawater - 2010:
11
12
13 571 Calculation and use of thermodynamic properties, Manual and Guides No. 56,
14
15 572 Intergovernmental Oceanographic Commission, UNESCO (English), available from:
16
17
18 573 <http://www.TEOS-10.org>.
19
20 574 Iriarte, J.L., González, H.E., Liu, K.K., Rivas, C., Valenzuela, C., 2007. Spatial and temporal
21
22 575 variability of chlorophyll and primary productivity in surface waters of southern Chile (41.5
23
24
25 576 - 43° S). Estuar. Coast. Shelf. Sci. 74, 471-480.
26
27 577 Iriarte, J.L., Pantoja, S., Daneri, G., 2014. Oceanographic Processes in Chilean Fjords of Patagonia:
28
29
30 578 From small to large-scale studies. Prog. Oceanogr. 129, 1-7.
31
32 579 Krock, B., Tillmann, U., John, U., Cembella, A.D., 2008. LC-MS-MS aboard ship: tandem mass
33
34
35 580 spectrometry in the search for phycotoxins and novel toxigenic plankton from the North
36
37 581 Sea. Anal. Bioanal. Chem. 392, 797-803.
38
39 582 Lelong, A., Hégaret, H., Soudant, P., Bates, S.S., 2012. *Pseudo-nitzschia* (Bacillariophyceae)
40
41
42 583 species, domoic acid and amnesic shellfish poisoning: revisiting previous paradigms.
43
44 584 Phycologia 51, 168-216.
45
46
47 585 León-Muñoz, J., Urbina, M.A., Garreaud, R., Iriarte, J.L., 2018. Hydroclimatic conditions trigger
48
49 586 record harmful algal bloom in western Patagonia (summer 2016). Sci. Rep. 8, 1330.
50
51
52 587 Lovegrove, T., 1960. An improved form of sedimentation apparatus for use with an inverted
53
54 588 microscope. J. Cons. Int. Explor. Mer. 25, 279-284.
55
56
57
58
59
60
61
62
63
64
65

- 1
2
3
4
5 589 Lundholm, N., Moestrup, Ø., Hasle, G.R., Hoef-Emden, K., 2003. A study of the *Pseudo-nitzschia*
6
7
8 590 *pseudodelicatissima/cuspidata* complex (Bacillariophyceae): what is *P.*
9
10 591 *pseudodelicatissima*? J. Phycol. 39, 797–813.
- 12
13 592 Margalef, R., 1978. Life forms of phytoplankton as survival alternatives in an unstable
14
15 593 environment. Oceanol. Acta 1, 493-509.
- 17
18 594 Margalef, R., Estrada, M., Blasco, D., 1979. Functional morphology of organisms involved in red
19
20 595 tides, as adapted to decaying turbulence in: Taylor, D., Seliger, H. (Eds.), Toxic
21
22 596 Dinoflagellate Blooms. Elsevier, New York, pp. 89-94.
- 25 597 Marshall, G.J., 2003. Trends in the southern annular mode from observations and reanalyses. J.
26
27 598 Climate 16, 4134–4143.
- 29
30 599 Molinet, C., Lafón, A., Lembeye, G., Moreno, C.A., 2003. Patrones de distribución espacial y
31
32 600 temporal de floraciones de *Alexandrium catenella* (Whedon & Kofoid) Balech 1985, en
33
34 601 aguas interiores de la Patagonia noroccidental de Chile. Rev. Chil. Hist. Nat. 76, 681-698.
- 37 602 Molinet, C., Niklitschek, E., Seguel, M., Díaz, P., 2010. Trends of natural accumulation and
38
39 603 detoxification of paralytic shellfish poison in two bivalves from the Northwest Patagonian
40
41 604 inland sea. Rev. Biol. Mar. Ocenog. 45, 195-204.
- 44 605 Montero, P., Daneri, G., González, H.E., Iriarte, J.L., Tapia, F.J., Lizárraga, L., Sanchez, N.,
45
46 606 Pizarro, O., 2011. Seasonal variability of primary production in a fjord ecosystem of the
47
48 607 Chilean Patagonia: Implications for the transfer of carbon within pelagic food webs. Cont.
49
50 608 Shelf. Res. 31, 202–215.
- 54 609 Montero, P., Daneri, G., Tapia, F., Iriarte, J.L., Crawford, D., 2017. Diatom blooms and primary
55
56 610 production in a channel ecosystem of central Patagonia. Lat. Am. J. Aquat. Res. 45, 999-
57
58 611 1016.

- 1
2
3
4
5 612 Pantoja, S., Iriarte, J.L., Daneri, G., 2011. Oceanography of the Chilean Patagonia. Cont. Shelf.
6
7
8 613 Res. 31, 149-153.
9
10 614 Pease, S.K.D., Brosnahan, M.L., Sanderson, M.P., Smith, J.L., 2022. Effects of two toxin-884
11
12 615 producing harmful algae, *Alexandrium catenella* and *Dinophysis acuminata*
13
14 616 (Dinophyceae), on activity and mortality of larval shellfish. Toxins 14, 335.
15
16
17 617 Pérez-Santos, I., Díaz, P.A., Silva, N., Garreaud, R., Montero, P., Henríquez-Castillo, C., Barrera,
18
19 618 F., Linford, P., Amaya, C., Contreras, S., Aracena, C., Pinilla, E., Altamirano, R., Vallejos,
20
21 619 L., Pavez, J., Maulen, J., 2021. Oceanography time series reveals annual asynchrony input
22
23 620 between oceanic and estuarine waters in Patagonian fjords. Sci. Total Environ. 798,
24
25 621 149241.
26
27
28 622 Pérez-Santos, I., Seguel, R., Schneider, W., Linford, P., Donoso, D., Navarro, E., Amaya-Cárcamo,
29
30 623 C., Pinilla, E., Daneri, G., 2019. Synoptic-scale variability of surface winds and ocean
31
32 624 response to atmospheric forcing in the eastern austral Pacific Ocean. Ocean Sci. Discuss.
33
34 625 15, 1247-1266.
35
36
37 626 Pickard, G.L., 1971. Some physical oceanographic features of inlets of Chile. J. Fish. Res. Board
38
39 627 Can. 28, 1077-1106.
40
41
42 628 Pinto-Torres, M., Pizarro, G., York, R.B., Alves-de-Souza, C., Lundholm, N., Mardones, J.I.,
43
44 629 Nariño, M.J., Iriarte, J.L., 2023. Unveiling species diversity within the toxic diatom genus
45
46 630 *Pseudo-nitzschia* from the fjords and channels of Magallanes (48°- 51°S), Chile. Prog.
47
48 631 Oceanogr. 211, 102957.
49
50
51 632 Pizarro, G., Montecino, V., Guzmán, L., Muñoz, V., Chacón, V., Pacheco, H., Frangópulos, M.,
52
53 633 Retamal, L., Alarcón, C., 2005. Patrones locales recurrentes del fitoplancton en fiordos y
54
55
56
57
58
59
60
61
62
63
64
65

1
2
3
4
5 634 canales australes (43°-56S°) en primavera y verano. Ciencia y Tecnología Marina 28, 63-
6
7
8 635 83.
9
10 636 Pizarro, G., Paz, B., Alarcón, C., Toro, C., Frangópulos, M., Salgado, P., Olave, C., Zamora, C.,
11
12 637 Pacheco, H., Guzmán, L., 2018. Winter distribution of toxic, potentially toxic
13
14 638 phytoplankton, and shellfish toxins in fjords and channels of the Aysén region, Chile. Lat.
15
16 639 Am. J. Aquat. Res. 46, 120-139.
17
18 640 Reynolds, C.S., Huszar, V., Kruk, C., Naselli-Flores, L., Melo, S., 2002. Towards a functional
19
20 641 classification of the freshwater phytoplankton. J. Plankton Res. 24, 417-428.
21
22 642 Rivera, P., 1985. Las especies del género *Nitzschia* Hassall, sección *Pseudonitzschia*
23
24 643 (*Bacillariophyceae*) en las aguas marinas chilenas. Gayana Bot. 42, 9-38.
25
26 644 Sauter, T., 2020. Revisiting extreme precipitation amounts over southern South America and
27
28 645 implications for the Patagonian Icefields. Hydrology and Earth System Sciences 24, 203-
29
30 646 2016.
31
32 647 Schneider, W., Pérez-Santos, I., Ross, L., Bravo, L., Seguel, R., Hernández, F., 2014. On the
33
34 648 hydrography of Puyuhuapi Channel, Chilean Patagonia. Prog. Oceanogr. 128, 8-18.
35
36 649 Smayda, T., Reynolds, C., 2001. Community assembly in marine phytoplankton: application
37
38 650 of recent models to harmful dinoflagellate blooms. J. Plankton Res. 23, 447-461.
39
40 651 Suárez-Isla, B.A., López-Rivera, A., Hernández, C., Clément, A., Guzmán, L., 2002. Impacto
41
42 652 económico de las floraciones de microalgas nocivas en Chile y datos recientes sobre la
43
44 653 ocurrencia de veneno amnésico de los mariscos, in: Sar, E., Ferrario, M.E., Reguera, B.
45
46 654 (Eds.), Floraciones Algales Nocivas En El Cono Sur Americano. Instituto Español de
47
48 655 Oceanografía, pp. 257–268.
49
50
51
52
53
54
55
56
57
58
59
60
61
62
63
64
65

- 1
2
3
4
5 656 Thomas, W., Gibson, C., 1990a. Effects of small-scale turbulence on microalgae. J. Appl. Physiol.
6
7
8 657 2, 71-77.
9
- 10 658 Thomas, W., Gibson, C., 1990b. Quantified small-scale turbulence inhibits a red tide dinoflagellate,
11
12 659 *Gonyaulax polyedra* Stein. Deep-Sea Research 37, 1583-1593.
13
14
- 15 660 Thomas, W., Vernet, M., Gibson, C., 1995. Effects of small-scale turbulence on photosynthesis,
16
17 661 pigmentation, cell division, and cell size in the marine dinoflagellate *Gonyaulax polyedra*
18
19 662 (Dinophyceae). J. Phycol. 31, 50-59.
20
21
- 22 663 Thompson, D.W., Wallace, J.M., 2000. Annular modes in the extratropical circulation. I. Month-
23
24 664 to-month variability. J. Climate 13, 1000–1016.
25
26
- 27 665 Torres-Palenzuela, J.M., González-Vilas, L., Bellas, F.M., Garet, E., González-Fernández, A.,
28
29 666 Spyarakos, E., 2019. *Pseudo-nitzschia* blooms in a coastal upwelling system: Remote
30
31 667 sensing detection, toxicity and environmental variables. Water 11, 1954.
32
33
- 34 668 Trainer, V.L., Bates, S., Lundholm, N., Thessen, A., Cochlan, W., Adams, N., Trick, C., 2012.
35
36 669 *Pseudo-nitzschia* physiological ecology, phylogeny, toxicity, monitoring and impacts on
37
38 670 ecosystem health. Harmful Algae 14, 271-300.
39
40
- 41 671 Utermöhl, H., 1958. Zur Vervollkommnung der quantitativen phytoplankton-Methodik. Mitt. Int.
42
43 672 Ver. Limnol. 9, 1-38.
44
45
- 46 673 Valenzuela, R.A., Garreaud, R., 2019. Extreme daily rainfall in central-southern Chile and its
47
48 674 relationship with low-level horizontal water vapor fluxes. Journal of Hydrometeorology 20,
49
50 675 1829-1850.
51
52
- 53 676 Valle-Levinson, A., 2010. Contemporary issues in estuarine physics Cambridge University Press
54
55 677 New York.
56
57
58
59
60
61
62
63
64
65

1
2
3
4
5
6
7
8
9
10
11
12
13
14
15
16
17
18
19
20
21
22
23
24
25
26
27
28
29
30
31
32
33
34
35
36
37
38
39
40
41
42
43
44
45
46
47
48
49
50
51
52
53
54
55
56
57
58
59
60
61
62
63
64
65

678 Valle-Levinson, A., Blanco, J., 2004. Observations of wind influence on exchange flows in a strait
679 of the Chilean inland sea. *J. Mar. Res.* 62, 721-741.

680 Viale, M., Garreaud, R., 2015. Orographic effects of the subtropical and extratropical Andes on
681 upwind precipitating clouds. *Journal of Geophysical Research - Atmospheres* 120,
682 10.1002/2014JD023014.

683 Viale, M., Valenzuela, R., Garreaud, R., Ralph, F., 2018. Impacts of atmospheric rivers on
684 precipitation in southern South America. *Journal of Hydrometeorology* 19, 1671–1687.

685

14
15
16
17
18
19
20
21
22
23
24
25
26
27
28
29
30
31
32
33
34
35
36
37
38
39
40
41
42
43
44
45
46
47
48
49
50
51
52
53
54
55
56
57
58
59
60
61
62
63
64
65

686

Table 1. Morphological characteristics of *Pseudo-nitzschia calliantha* found in Chile and Denmark.

Author	Year	Locality	Fibula/10 μm	Inter-striae/10 μm	Central interspace	Rows of poroids (n)	Poroids/ 1 μm	Apical axis (μm)	Transapical axis (μm)	Evaluated cells (n)
Lundholm et al.	2003	Denmark	15–21	34–39	+	1	4 -6	41–98	1.3–1.8	
Álvarez et al.	2009	Northern Chile	15–22	34–39	+	1	4–8	41–98	1.3–1.8	
Pinto-Torres et al.	2023	Southern Chile	18–22	36–39	+	1	4–6	65–80	1.9–2.3	6
This study	2023	Southern Chile	18–22	36–39	+	1	4–6	65–80	1.3–1.8	
			(20.4 \pm 1.8)	(38 \pm 1.2)			(4.9 \pm 0.9)	(74.8 \pm 5.9)	(1.5 \pm 0.2)	10

687

1
2
3
4
5
6
7
8
9
10
11
12
13
14
15
16
17
18
19
20
21
22
23
24
25
26
27
28
29
30
31
32
33
34
35
36
37
38
39
40
41
42
43
44
45
46
47
48
49
50
51
52
53
54
55
56
57
58
59
60
61
62
63
64
65

688 **Figure legends**

689 **Figure 1.** Map showing: A) Chile (the box delimits Northwest Patagonia); B) Northwest Patagonia
690 (the box delimits Puyuhuapi Fjord); C) Puyuhuapi Fjord and Magdalena Sound. The red
691 circle indicates the sampling station.

692 **Figure 2.** Regional and hemispheric conditions in early 2018. Maps of precipitation anomalies
693 over southern Chile for (A) January–February and (B) March–April 2018. The
694 anomalies are the bi-monthly average minus the long-term mean, divided by the long-
695 term mean, expressed as a % (data source: CR2Met). The globe inset shows the surface
696 pressure anomalies (departure from the long-term mean, in hPa) for the corresponding
697 months. (C) Average Southern Annular Mode (SAM) index (hPa) for January–February
698 and March–April. The values for 2018 are highlighted by the red line.

699 **Figure 3.** Left panels: Time series (every 6 hr) from ERA5 data interpolated for Magdalena Island
700 (45°S, 73°W) from January 1 to April 30, 2018. From top to bottom: (A) Precipitation
701 rate (mm/6 hr), (B) 850 hPa (~1500 m ASL) zonal wind (west to east, m/s) and (C) 850
702 hPa air temperature (°C). In (b) and (c), the horizontal line is the seasonal average.
703 Periods of stronger westerlies/colder temperatures are shown in blue, and periods of
704 weaker westerlies/warmer temperatures in orange. Right panel (D): Image (MODIS
705 Terra True Color) obtained around midday of March 8, 2018, showing an atmospheric
706 river (AR) making landfall in northern Patagonia. The semi-transparent shading is the
707 24-hr accumulated precipitation determined by the IMERG satellite product (light rain
708 in green, heavy rain in yellow). The blue arrow indicates the predominant WSW flow in

1
2
3
4
5 709 the lower and middle troposphere, signaling the marked contrast between cold air to the
6
7
8 710 south and warm air to the north of the AR.
9

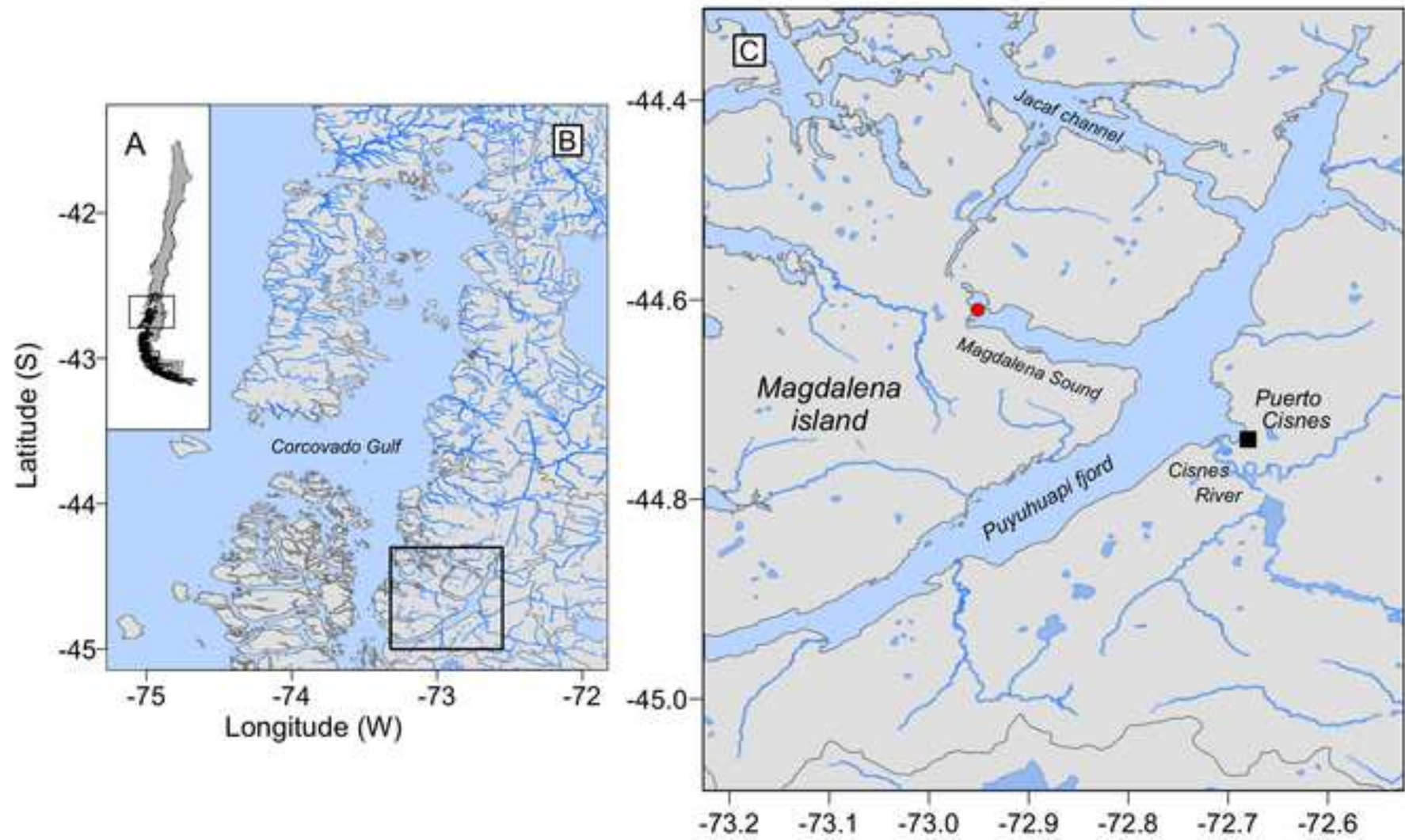
10 711 **Figure 4.** Vertical distribution of A) conservative temperature ($^{\circ}\text{C}$); B) absolute salinity (g kg^{-1});
11
12 712 Brunt-Väisälä frequency (cycles h^{-1}); D) dissolved oxygen (mL L^{-1} and % saturation)
13
14
15 713 and dissolved oxygen (mL L^{-1}); E) pH and F) fluorescence (Volts, from 0 to 50) at a
16
17 714 fixed sampling station at the head of Magdalena Sound from January to April 2018.
18
19

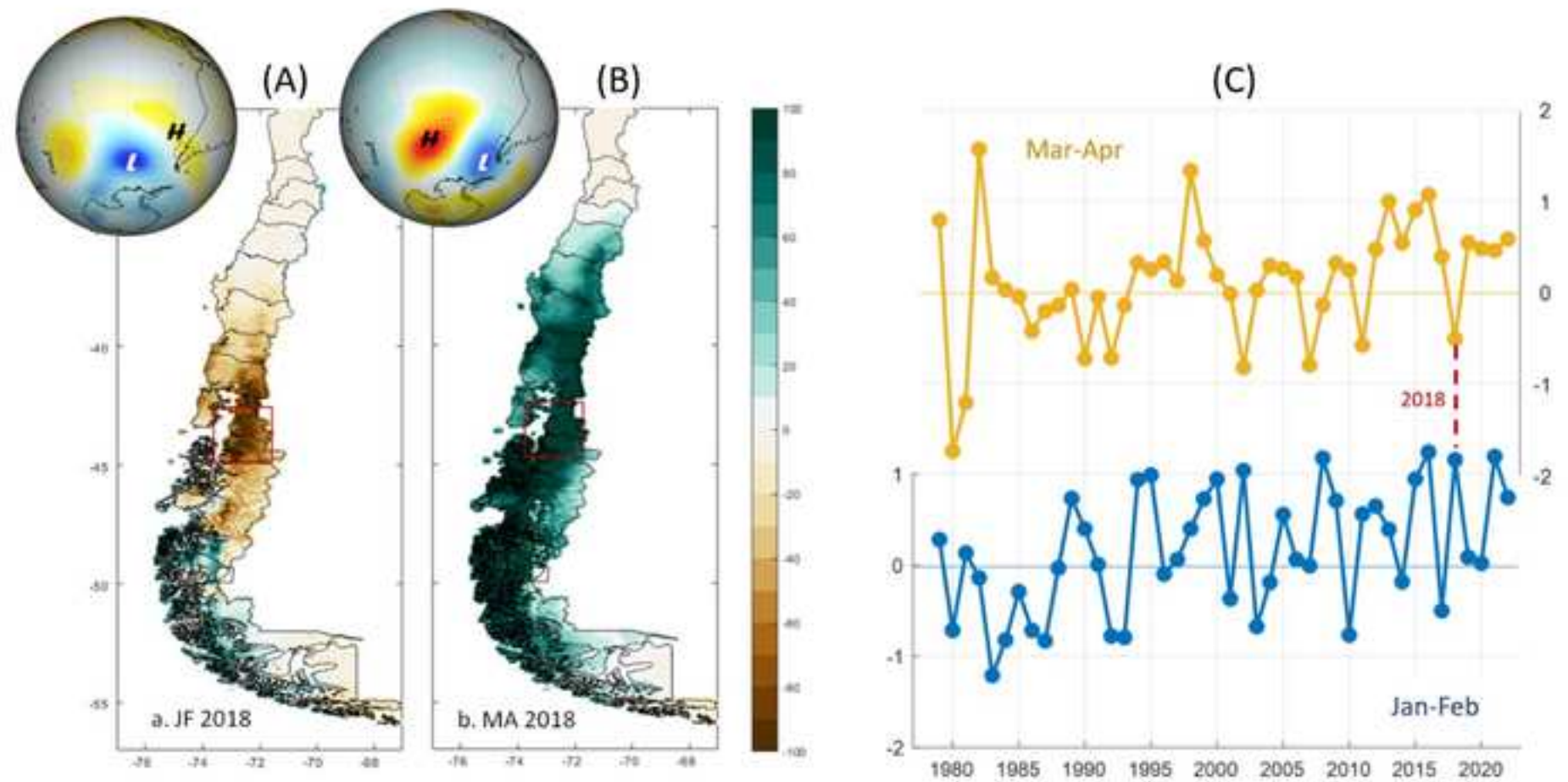
20 715 **Figure 5.** Vertical distribution (0–20 m) of: **upper panel:** temperature (blue line), salinity (red
21
22 716 line) and fluorescence (green line); **middle panel:** cell density (cells L^{-1}) of *Dinophysis*
23
24
25 717 *acuta* (orange circles) and *Pseudo-nitzschia calliantha* (green circles); **lower panel:**
26
27 718 Percentage of the total phytoplankton contribution (%) at a fixed sampling station on A)
28
29
30 719 January 17, B) February 16, C) March 12 and April 23, 2018.
31

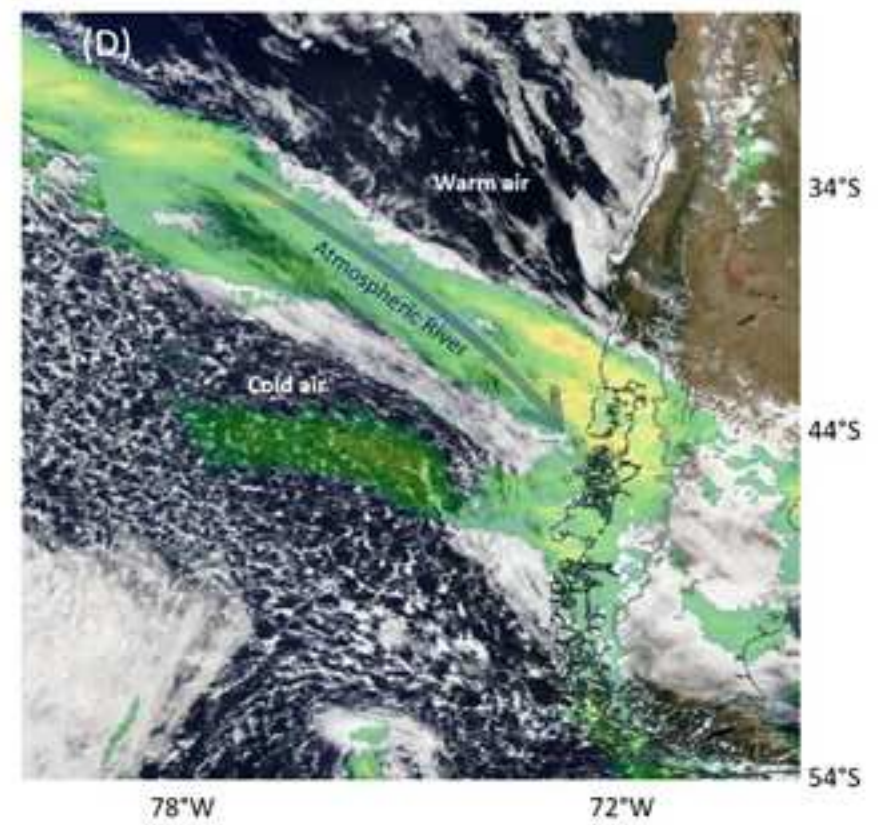
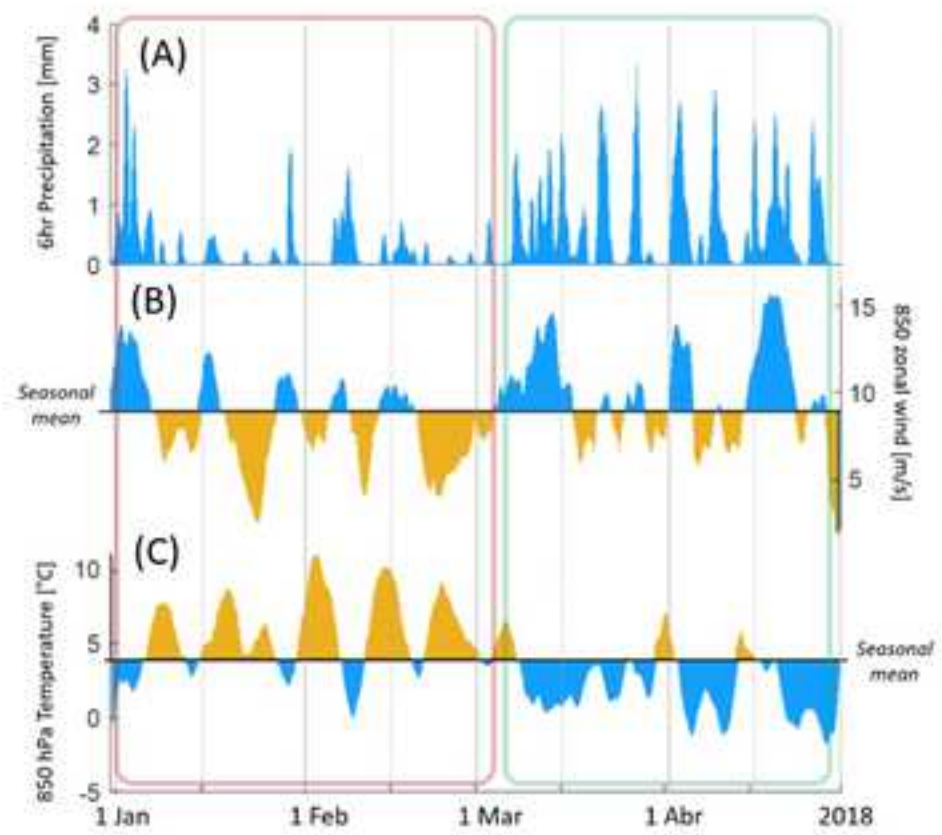
32 720 **Figure 6.** Toxin contents determined in vertical net hauls from February 16 and March 12, 2018.
33
34 721 The green bar indicates domoic acid and blue shades indicate lipophilic toxins. ND =
35
36
37 722 not detected.
38

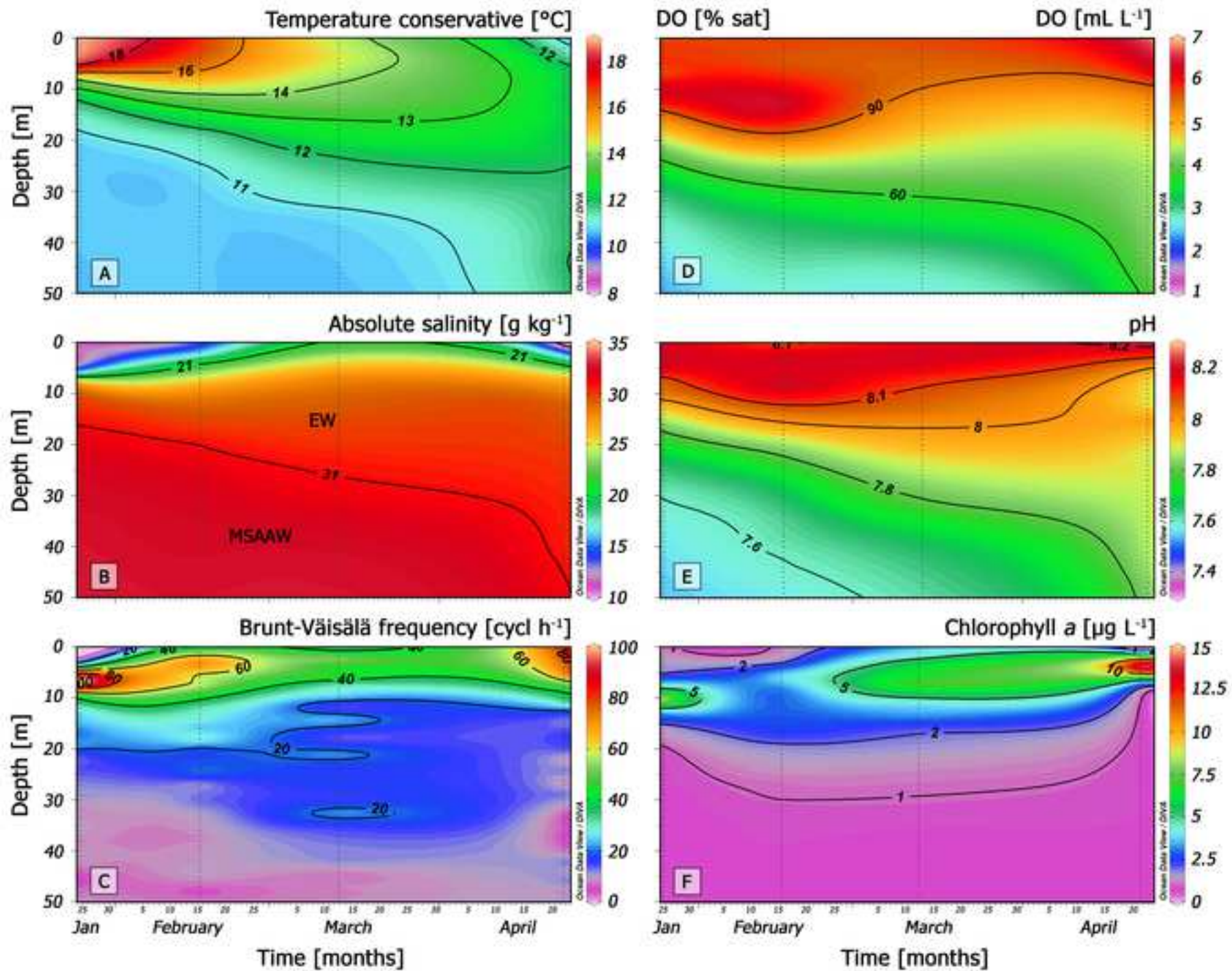
39 723 **Figure 7.** Scanning electron microscopy image of *Pseudo-nitzschia calliantha* isolated from
40
41
42 724 Magdalena Sound during a bloom in February 2018.
43

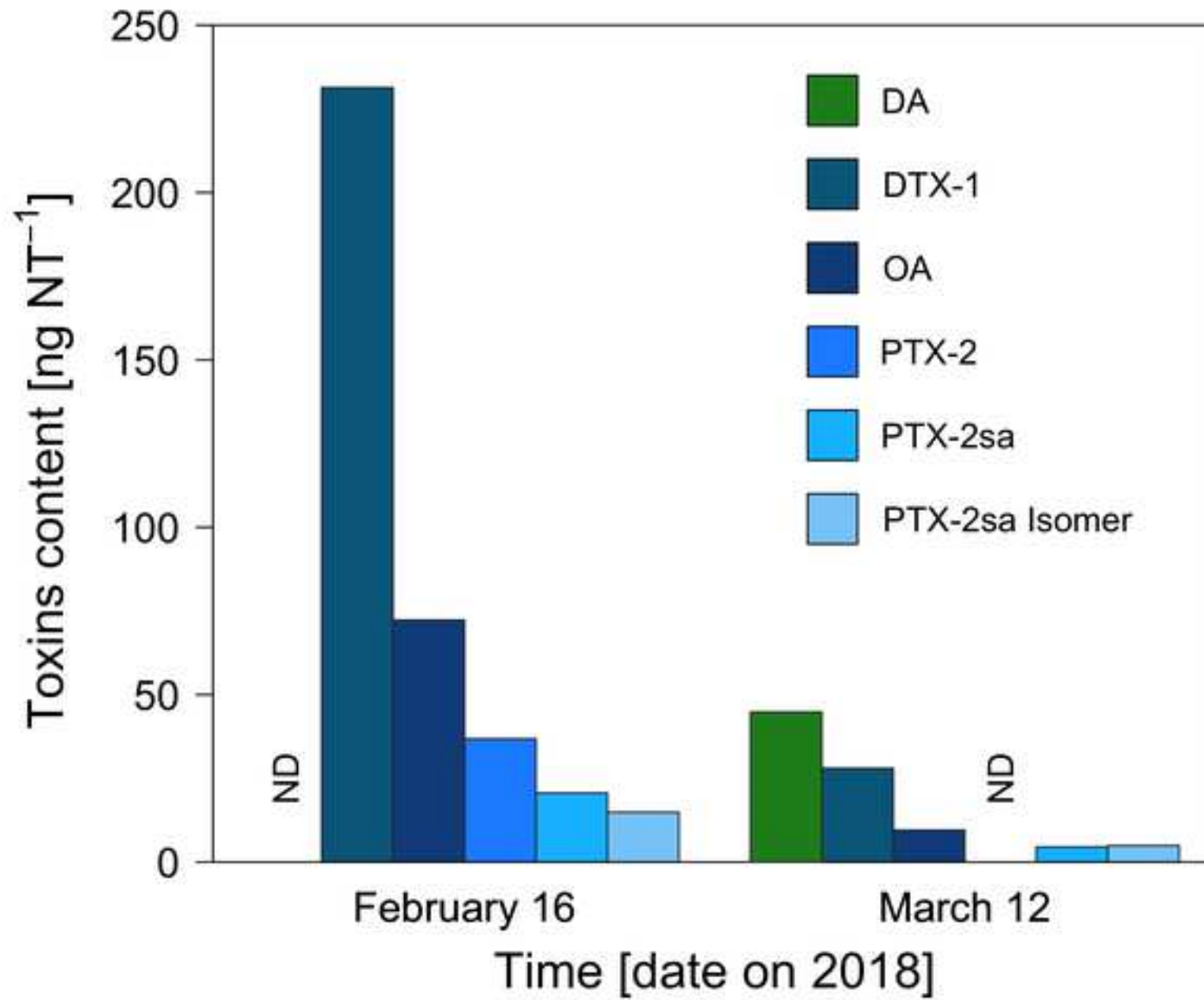
44 725 **Figure S1.** Selected reaction monitoring chromatograms shown the transitions m/z 312/266 and
45
46
47 726 312/161 of: A) a standard solution of domoic acid (DA) and B) a phytoplankton net
48
49 727 sample from Magdalena Sound on March 12, 2018.
50
51
52
53
54
55
56
57
58
59
60
61
62
63
64
65

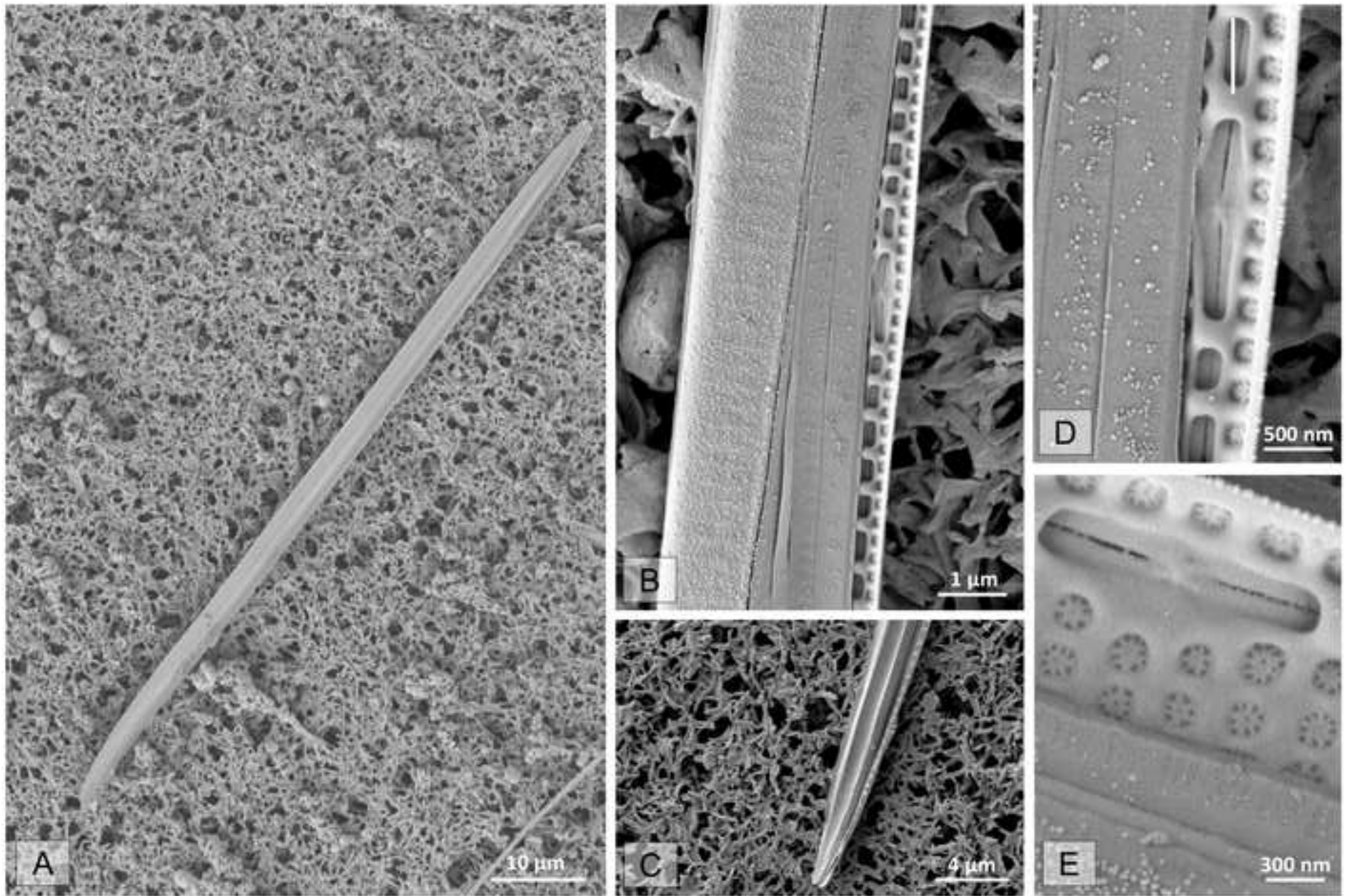


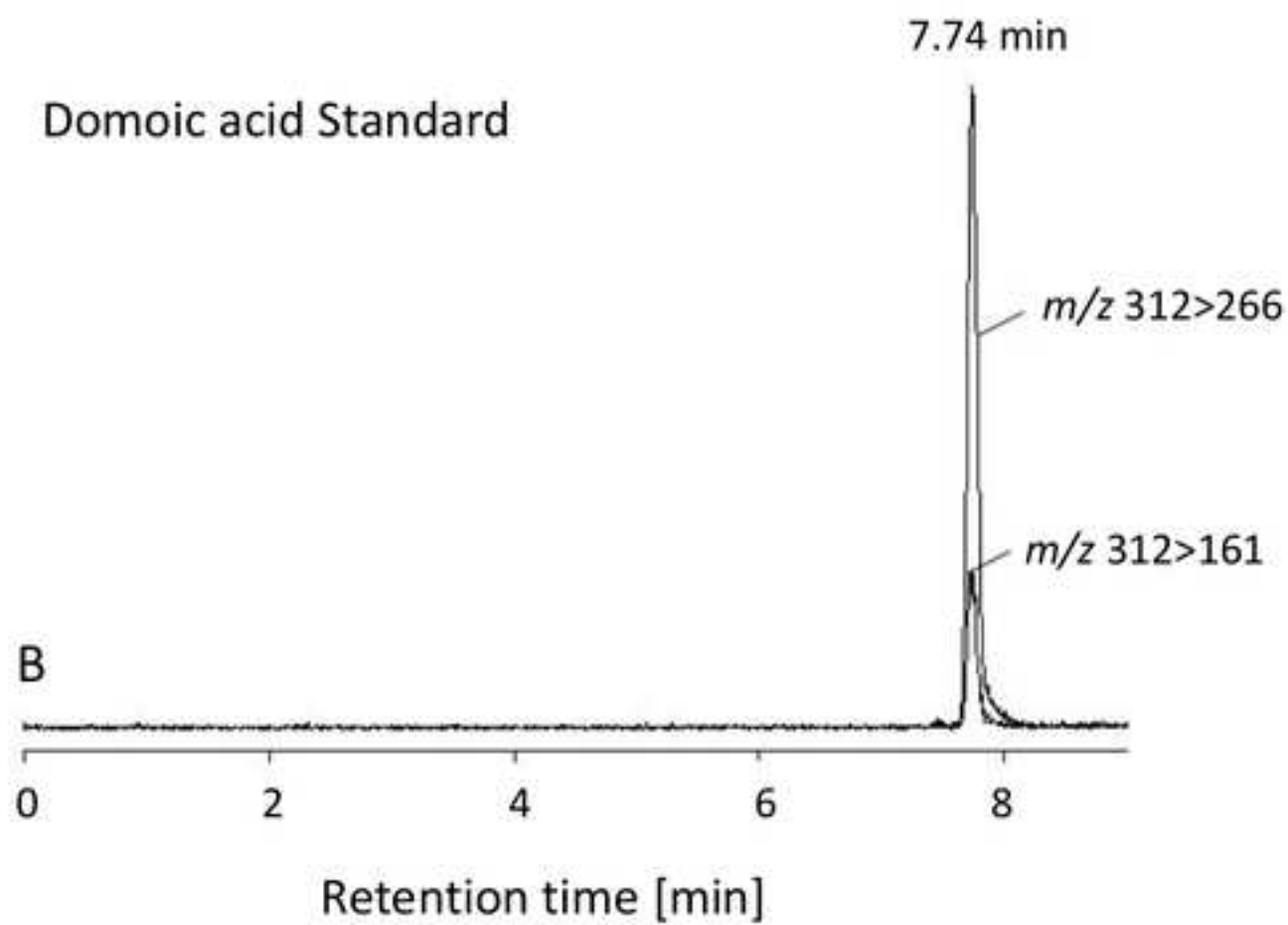
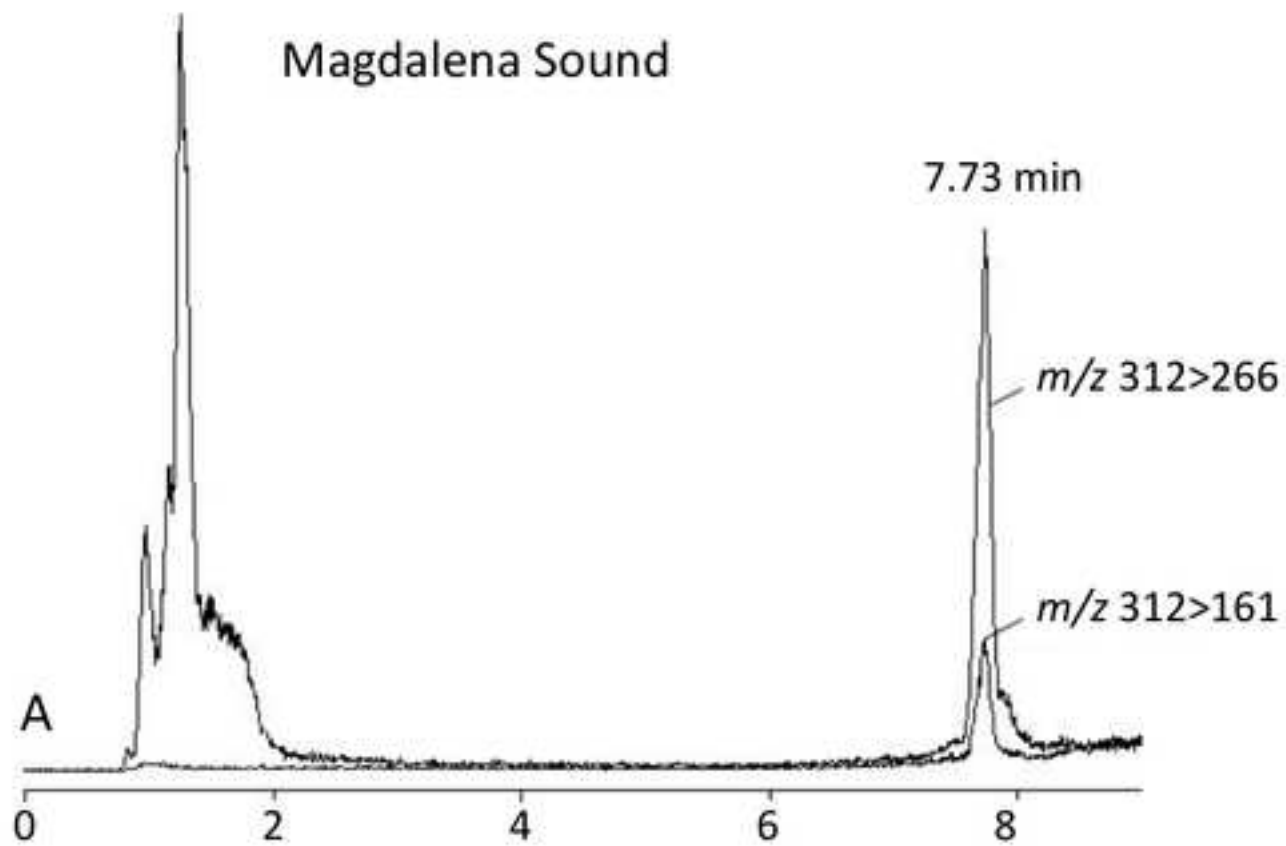












Declaration of interests

The authors declare that they have no known competing financial interests or personal relationships that could have appeared to influence the work reported in this paper.

The authors declare the following financial interests/personal relationships which may be considered as potential competing interests:

We have not financial interests/personal relationships which may be considered as potential competing interests.